Characterisation of Redox States of Metal-Organic Frameworks by Growth on Modified Thin-film Electrodes

Tamoghna Mitra,[a,b] Florian Moreau,[a,c] Adam Nevin,[a,c] Carlo U. Perotto,[a] Alex Summerfield,[d] E. Stephen Davies,[a] Elizabeth A. Gibson,[a,e] Timothy L. Easun,[a,f,*] and Martin Schröder[a,b*]

a. School of Chemistry, The University of Nottingham, University Park Nottingham, NG7 2RD, UK

b. Department of Chemistry, The University of Liverpool, Crown Street, Liverpool, L69 7ZD, UK

c. School of Chemistry, The University of Manchester, Oxford Road, Manchester M13 9PL, UK

d. School of Physics and Astronomy, The University of Nottingham, University Park Nottingham, NG7 2RD, UK

e. School of Chemistry, Bedson Building, Newcastle University, Newcastle upon Tyne NE1 7RU, UK

f. School of Chemistry, Cardiff University, Park Place, Cardiff, CF10 3AT, UK

† Footnotes relating to the title and/or authors should appear here.

Electronic Supplementary Information (ESI) available: [details of any supplementary information available should be included here]. See DOI: 10.1039/x0xx00000x

Abstract

The application of metal-organic framework (MOF) materials in electrochemical and electrochromic devices remain rare. One of the main reasons for this is the inability to readily access their detailed electrochemistry. The inherent insolubility of these materials does not allow interrogation by traditional solution-based electrochemical or spectroscopic methods. In this study, we report a straightforward alternative approach to the spectroelectrochemical study of MOFs. We have used two systems as exemplars in this study, MFM-170 and MFM-180. The method involves chemical modification of a working electrode to attach MOF materials without using corrosive reagents such as inorganic acids or bases which otherwise could limit their application in device development. MFM-170 demonstrates the formation of a stable radical species $[MFM\text{-}170]^{\bullet+}$ on electrochemical oxidation, and this has been characterised by electrochemical, spectroelectrochemical and EPR spectroscopic techniques coupled to DFT analysis.

Introduction

The last decade has seen enormous progress in the field of self-assembled porous materials,[1] particularly of crystalline, microporous metal-organic framework (MOF) materials.[2, 3] The crystalline nature of MOF materials enables their study by X-ray crystallographic methods,[4] and their high porosity and internal surface areas are properties which have been exploited for storage, separation and mass transfer[5-95-95-9] applications.[10, 11] More recently MOFs have been considered in electrocatalysis[12-14] and in electrochromic devices,[15, 16] and there are also a few reports on light-induced modification of both MOF structures and redox properties.[17-22] However, there remain significant obstacles in this area particularly with regard to the insulating nature of many framework systems, and detailed studies into the redox activity of MOFs remain scarce due mainly to the insolubility of MOF materials and the lack of general, straightforward methods to study MOFs in their non-native redox states.[23-25] One way to address this scarcity is to combine reaction-oriented bulk electrolysis of MOFs with species-focused *in situ* spectroscopic methods such as UV-Vis or IR absorption spectroscopies. A key challenge here is to prepare an optically transparent electrode (OTE) modified/coated with a thin film of MOF to allow spectroelectrochemical characterisation of redox processes leading potentially to exploitation of electrochromic effects.

Attempts have been made to elucidate the spectral properties of MOFs in their redox accessible states using *in situ* UV-Vis-NIR spectroelectrochemical techniques.[26] One approach is to affix crystalline MOF particles onto an optically transparent indium-doped tin oxide electrode (ITO) using an electrolyte intercalated polyvinylchloride as a form of mechanical 'glue'.[26] Though the simplicity of this route makes it a powerful method for studying the redox properties of MOFs, the reliability of contact between conducting surface and mechanically affixed MOF crystals can be an issue. Solvothermal synthesis of a redox active and optically transparent thin film of a water-stable pyrazolate-based MOF bound to a conducting fluorine-doped tin oxide (FTO) coated glass has been reported.[16] The key feature

of this route is the strong adhesion of the pyrazolate-based crystals to the FTO surface. Unfortunately, most MOF crystals do not tend to adhere strongly to surfaces without external modification, making current methods applicable to only specific MOFs. Moreover, many MOF syntheses require the presence of corrosive acid or base which can harm the conductive surface. We, therefore, devised an alternative path to synthesise a thin film of MOF on a transparent conducting surface. Synthesis of surface mounted MOF films, so-called SURMOF, has been reported whereby solutions of structural components are deposited sequentially onto non-transparent functionalized gold substrates *via* a 'layer-by-layer' (LBL) growth method.[27-29] The resulting films are often described as ultra-thin, oriented, and thickness adjustable, although the uniformity of the SURMOF layers and controllability of the growth are not always entirely clear cut.[30] Despite this, the generality and simplicity of this sequential deposition approach has allowed us to synthesis a MOF film onto a modified electrode. We report herein the synthesis and electrochemical properties of MOF films containing redox-active organic linkers on the conducting platforms of ITO-glass and carbon paper.

We have long been concerned with the development of modular syntheses for Cu(II) paddlewheel MOFs with poly-aromatic, highly conjugated organic linkers at their core.[31] One such family of frameworks are based on Cu(II) paddlewheel nodes with octa- and tetra-carboxylate ligands.[33] For the current study, we chose frameworks containing redox active 9,10-phenylanthracene (H_4L^1) in MFM-170 [32] and tetraphenylethylene (H_8L^2) in MFM-180 (also known as PCN-922) (Figure 1). Both MOFs can be synthesised as crystalline powders by heating Cu(II) salts with the organic ligand in N, N-dimethylformamide (DMF) at 80 °C in a sealed tube. MFM-170 crystallises in orthorhombic space group *Imma*, while MFM-180 crystallises in tetragonal space group *I-42m*. Both framework systems have paddlewheel units linked by tetracarboxylate (MFM-170)[32] or octacarboxylate (MFM-180)[33, 34] linkers to form porous 3D lattices.

Results and Discussion

Synthesis of modified electrode

To grow a film of each MOF on ITO-coated glass or carbon paper the conducting platform needs to be functionalized. For this purpose, electrode surfaces were coated with a monolayer of 4-phenyl carboxylic or 3,5-phenyl dicarboxylic acid *via* electrodeposition of 4-carboxylic- or 3,5-dicarboxlic-phenyl diazonium cations (Figure S1).[35] These diazonium cations were chosen to match the end group of the corresponding ligand. Thus, to grow MFM-170 the 4-carboxylic phenyl diazonium salt was used, and for MFM-180 the 3,5-dicarboxlic phenyl diazonium salt was chosen (Figure 2). The efficient functionalization of the surface can be monitored by measuring the conductivity of the surface, before and after functionalization. Formation of an aryl-monolayer blocks the surface and slows down the electron transfer processes between the electrolyte solution and the underlying conductive surface. This blocking effect is demonstrated for our samples by electrochemical impedance spectroscopic measurements. We found that the formation of MOF could be readily achieved by sequentially immersing the functionalized surface in DMF solutions of metal salts and ligand, rather than by the normal solvothermal synthesis in a sealed vessel. Between each immersion, the surface was washed with DMF to remove unreacted reagents. These immersion cycles were repeated (10, 15, 20 or 50 times) to obtain films of different thicknesses. The immobilisation of these films was demonstrated by their resilience to multiple washings in a range of organic solvents (DMF, CH_2Cl_2, CH_3CN) or to sonication in CH_2Cl_2. We attribute this resilience to the covalent linkage between MOF and surface afforded by the electrodeposited aryl monolayer acting as "covalent glue".

As anticipated,[36, 37] PXRD of these films confirms their crystalline nature, with the peak intensities strongly suggesting there is a high degree of preferred orientation in the films (Figure S7). Unsurprisingly, atomic force microscopy (AFM) indicates their thickness increases with increasing numbers of immersion cycles.[38, 39] However, AFM images indicate

that these films consist of aggregates of nano crystals rather than the coverage that might be expected from pure epitaxial type growth (Figure S6). This is unsurprising given the relatively rough surfaces afforded by ITO and carbon paper electrodes. As shown by AFM (Figure S6) the MFM-180 film is made of continuous packing of MOF crystallites. MFM-170, however, forms a discontinuous film made of isolated islands of agglomerated crystallites.

Electrochemical and DFT analysis

Our ability to grow thin films of highly oriented, covalently-bound thin MOF films encouraged us to explore the electrochemical behaviour of the films. Cyclic voltammetry (CV) measurements were carried out in CH_2Cl_2 solutions containing $[^nBu_4N][BF_4]$ (0.4 M) as supporting electrolyte using a three-electrode electrochemical cell comprising of a platinum wire as the counter electrode, an Ag/AgCl (sat. KCl) as reference electrode and the MOF films grown on carbon paper acting as the working electrode. For cyclic voltammetry, the films grown on carbon paper were used as working electrodes primarily due to the superior conductivity of the carbon paper over ITO-coated glass. Conversely, the ITO-based films were used as working electrodes for subsequent spectroelectrochemical studies to exploit the transparent nature of the ITO-coated glass. Prior to any electrochemical study, the guest DMF within the framework pores was exchanged with CH_2Cl_2. The films were conditioned by soaking in the electrolyte solution for 24-48 h to allow maximum electrolyte diffusion into the pore structure prior to the electrochemical experiment. The cyclic voltammograms of each MOF film and those of solutions of ethyl esters of their corresponding ligands in solution in CH_2Cl_2 are shown in Figure 3. Each film exhibited well-defined redox behaviour consistent with oxidation of MOF frameworks, described further below.

The MFM-170 film showed a reversible process at $E_{1/2}$ = 0.75 V (*vs* Fc^+/Fc) The observed peak separations (ΔE = 28 mV at 5 mV/s scan rate) and the relationship between the peak currents and scan rate (i α scan rate$^{0.82}$) suggests that the system is neither completely diffusion controlled (ideally ΔE = 59 mV, i α scan rate$^{0.5}$) nor

surface-confined (ideally ΔE = 0 mV, i α scan rate). The effects of mass transfer limitations within the film due to hindered diffusion, as might also be expected for porous, non-conductive films,[40] are also visible (see Figure S8 and related discussion for additional details). CV measurements in solution for the ethyl ester Et_4L^1 on a glassy carbon electrode showed a reversible oxidation process at $E_{1/2}$ = 0.88 V (Figure 3). This was shown to be a one electron oxidation process by coulometry. The slight cathodic shift of the oxidation process in the MOF film relative to Et_4L^1 is consistent with greater negative charge density on the deprotonated ligand in the MOF framework. Notably, the MFM-170 film also showed excellent stability to electrochemical cycling with no decrease in the peak current observed over multiple cycles at scan rates between 2 and 10 mV/s. In contrast, the octaester Et_8L^2 shows two oxidation processes at $E_{1/2}$ = 0.92 V and E_p^a = 1.11 V, the latter not demonstrating a return wave in the return cycle at the scan rates employed. We attribute the first process to the formation of a tetra-phenyl ethylene based radical ion.[41] This behaviour differs from that of MFM-180 film which displays only an irreversible process (E_p^a = 0.92 V).

Table 1: Summary of cyclic voltammetric data.

	Et_4L^1	**MFM-170**	**Et_8L^2**	**MFM-180**
*$E_{1/2}$ (V)	0.875	0.75	0.92	-
*E_p^a (V)	-	-	1.11	0.92

*$E_{1/2}$ = (E_p^a + E_p^c)/2, E_p^a = peak potential of the anodic peak; E_p^a = peak potential of the cathodic peak

Bulk electrochemical and DFT analysis of MFM-170

To understand these redox processes in detail we decided to monitor each process using UV-Vis absorption spectroscopy (Figure 4a,b). The spectral changes in the MOF films were compared with those observed for the solutions of the ester derivatives of the corresponding ligand in the same electrolyte solution. During this study, the working electrode was fixed at a constant overpotential to achieve the desired redox reaction, while UV-Vis absorption spectra were collected at regular time intervals. The spectral changes observed due to oxidation of Et_4L^1 at 1.14 V are characterised by the disappearance of π–π* transitions of the neutral species around $\lambda_{max} \approx 350–410$ nm concomitant with the appearance of new absorption bands around $\lambda_{max} \approx 550–700$ nm assigned to π–π* transitions of the oxidized species. This suggests the formation of a ligand-centred radical cation species.[41] The presence of an isosbestic point at $\lambda_{iso} \approx 410$ nm indicates that the electrochemical oxidation of Et_4L^1 is reversible, occurring without involving any chemical degradation. Furthermore, the chemical stability of the oxidised species under these conditions was confirmed by the regeneration of the spectral profile of the starting material Et_4L^1 upon application of potential sufficiently negative to reduce the oxidised species. The oxidation of films of MFM-170 displays similar behaviour to those above, albeit that the bands are slightly red shifted, consistent with the observed oxidation of the MOF being ligand-centred.

The first oxidation of a molecular system is often considered to be directly related to the energy of the highest occupied molecular orbital (HOMO) of that system. Therefore, to better understand the nature of the oxidation process of Et_4L^1 and to support the above assignment that the oxidation in the MOF is ligand-centred we have carried out density-functional-theory (DFT) calculations to identify the HOMO. The calculated HOMO for Et_4L^1 is almost entirely centred on the anthracene moiety (Figure 4c), a result that is unsurprising given the similarity of the UV-Vis absorption spectrum to that of many other anthracene-bearing molecules.[41] To compare the orbital character of the valance band of MFM-170 with the HOMO for Et_4L^1, a simplified model of MFM-170 was considered. The model consisted of four Cu(II)

paddlewheel clusters connected *via* one ligand and truncated by benzoate ions. The DFT calculations for this model show that the HOMO within MFM-170 is anthracene-based (Figure 4d) supporting the oxidation of MFM-170 being ligand-centred.

Bulk electrochemical analysis of MFM-180

Changes in the UV/Vis spectrum of Et_8L^2 upon oxidation (at 1.0 V) are characterised by the disappearance of π–π* transitions of the neutral species around $\lambda_{max} \approx 350–410$ nm (Figure 5). The disappearance of this band coincides with the appearance of a new absorption feature around $\lambda_{max} \approx 600$ nm indicating the formation of a radical cation species.[41] However, in this case, no isosbestic points were observed during the progress of the oxidation. Furthermore, the starting material was not regenerated completely upon reduction of the oxidised species indicating instability of the electrogenerated radical ion.

As expected, the MFM-180 film shows similar spectral behaviour to Et_8L^2 upon oxidation (0.95 V). Oxidation results in the disappearance of the π–π* transition band at 350-410 nm and the concomitant formation of a band at ~625 nm in the UV-Vis absorption spectrum attributed to the generation of a radical cation species. However, the oxidised MFM-180 film during these experiments degrades with loss of the band at 625 nm. This is illustrated by a plot of the changes in absorbance at 355 nm and 625 nm against time (Figure 6e) suggesting that that the radical cation $[MFM\text{-}180]^{\bullet+}$ decomposes, possibly via a non-redox chemical transformation.[40] This is in contrast to the spectroelectrochemical investigation of $[MFM\text{-}170]^{\bullet+}$, generated *via* electrochemical oxidation of MFM-170, which shows the radical cation to be stable. The concentration of this radical species can be controlled by switching the bias on-off (Figure 6c).

EPR analysis of [MFM-170] $^{\bullet+}$

To better understand the nature of the SOMO of oxidized MFM-170, we recorded EPR spectra of oxidized Et_4L^1 (*i.e.*, $[Et_4L^1]^{\bullet+}$) as a fluid solution and MFM-170 (*i.e.*, [MFM-170]$^{\bullet+}$) powder, each at ambient temperature. The radical cation of Et_4L^1 was generated electrochemically in CH_2Cl_2 solution whilst the oxidation of the MOF was achieved chemically using $NOBF_4$ [42] as the oxidant. The experimental EPR spectrum of oxidized Et_4L^1 can be reasonably reproduced by simulation using the hyperfine couplings of three sets of equivalent protons (g_{iso} = 2.0027, a_{4H} 2.553 x 10^{-4} cm^{-1}, a_{4H} 1.161 x 10^{-4} cm^{-1}, a_{6H} 0.382 x 10^{-4} cm^{-1}). This suggests that the SOMO for $[Et_4L^1]^{\bullet+}$ is localised mainly on anthracene core but some electron density is delocalised onto the two adjoining 3,5-substituted phenyl rings (Figure 6, Figure S10 and related discussion). Although we failed to resolve hyperfine coupling in oxidized MFM-170 powder, g_{iso} values are consistent with an organic based radical and the spectral width is similar to that of $[Et_4L^1]^{\bullet+}$ suggesting a common location for the SOMO.

In order to explain the difference in stability between [MFM-170]$^{\bullet+}$ and [MFM-180]$^{\bullet+}$ we note that in the crystal structure of MFM-170 the 9- and 10-positions of the anthracene (the reactive part of the anthracene core) are sterically crowded (Figure 6d) which may make the radical cation [MFM-170]$^{\bullet+}$ kinetically more stable to nucleophilic attack. The redox active 'tetraphenylethylene' core in MFM-180 lacks this protection which makes [MFM-180]$^{\bullet+}$ more susceptible to attack by any nucleophile present. We, therefore, suggest that presence of any water or other nucleophilic guest trapped in the MOF framework scavenges the radical in [MFM-180]$^{\bullet+}$. Although in principle a ligand-ligand dimerization reaction pathway is also possible, we propose that such a pathway may not be favourable due to the long ligand-ligand distance in the crystal structure (Figure S14).[43]

Unfortunately, when attempting to study the reduction properties of MFM-170 and MFM-180 both samples underwent film delamination. This was not entirely unexpected since reductions based either at the Cu(II) centres or the carboxylates may demand significant alterations in

the coordination geometry of the metal nodes which could destabilise the frameworks and lead to delamination of the film.

Conclusions

A method of generating surface bound MOFs to study their electrochemical properties has been developed and has been described for two samples. Both MFM-180 and MFM-170 can be oxidized to generate radical cationic species, $[MFM\text{-}180]^{\bullet+}$ and $[MFM\text{-}170]^{\bullet+}$, respectively. Though $[MFM\text{-}180]^{\bullet+}$ is unstable, $[MFM\text{-}170]^{\bullet+}$ is stable to redox cycling**.** The methodology outlined in this work allows for the design of new materials for electrocatalysis [44] and provides a framework by which such materials may be studied using *in situ* spectroscopic methods. The success of this spectro-electrochemical approach relies on our technique of covalently attaching stable MOF films on conducting working electrode surfaces *via* functionalization of the surface with a "chemical glue" onto which can be attached a thin film of MOF. Covalent attachment allows the MOF framework to be securely attached on to an electrode surface (subject to their chemical degradation). It has been previously shown that electrons are transferred between electrode and substrate through immobilized conjugated “molecular bridges” much rapidly than in the absence of such bridges.[40,45] In the present case, the immobilized contact between substrate (MOF) and electrode is likely to favour electron transfer between them. This also circumvents reliance upon deposition of material onto a surface by mechanical means. The covalently-bound, surface-modifying carboxylate species is likely to affect the orientation and growth of MOF crystallites on a surface, an area in which our investigations are ongoing. Also, this method does not involve corrosive reagents, for example, inorganic acids often needed for MOF synthesis, which may harm fragile and costly conducting surfaces. This new approach can potentially open up a new pathway to fabricate MOF-modified electrodes or semiconductor based devices.

Acknowledgements

We thank the U.K. Engineering and Physical Sciences Research Council for funding (Grant EP/I011870/1). M.S. thanks the European Research Council for support from an Advanced Grant (AdG 226593). TLE gratefully acknowledges the Royal Society for the award of a University Research Fellowship. EAG gratefully acknowledges the Royal Society for the award of a Royal Society Dorothy Hodgkin Fellowship.

Notes and references

1. A. G. Slater and A. I. Cooper, *Science*, 2015, **348**.
2. J. R. Long and O. M. Yaghi, *Chem. Soc. Rev.*, 2009, **38**, 1213-1214.
3. H.-C. Zhou, J. R. Long and O. M. Yaghi, *Chem. Rev.*, 2012, **112**, 673-674.
4. M. Li, D. Li, M. O'Keeffe and O. M. Yaghi, *Chem. Rev.*, 2014, **114**, 1343-1370.
5. S. Yang, A. J. Ramirez-Cuesta, R. Newby, V. Garcia-Sakai, P. Manuel, S. K. Callear, S. I. Campbell, C. C. Tang and M. Schröder, *Nat. Chem.*, 2015, **7**, 121-129.
6. Z. R. Herm, B. M. Wiers, J. A. Mason, J. M. van Baten, M. R. Hudson, P. Zajdel, C. M. Brown, N. Masciocchi, R. Krishna and J. R. Long, *Science*, 2013, **340**, 960-964.
7. H. Furukawa, K. E. Cordova, M. O'Keeffe and O. M. Yaghi, *Science*, 2013, **341**.
8. Y. Yan, X. Lin, S. Yang, A. J. Blake, A. Dailly, N. R. Champness, P. Hubberstey and M. Schroder, *Chem. Commun.*, 2009, 1025-1027.
9. S. Bureekaew, S. Horike, M. Higuchi, M. Mizuno, T. Kawamura, D. Tanaka, N. Yanai and S. Kitagawa, *Nat. Mater.*, 2009, **8**, 831-836.
10. H. B. Tanh Jeazet, C. Staudt and C. Janiak, *Dalton Transactions*, 2012, **41**, 14003-14027.
11. M. Shah, M. C. McCarthy, S. Sachdeva, A. K. Lee and H.-K. Jeong, *Ind. Eng. Chem. Res.*, 2012, **51**, 2179-2199.
12. L. Yang, S. Kinoshita, T. Yamada, S. Kanda, H. Kitagawa, M. Tokunaga, T. Ishimoto, T. Ogura, R. Nagumo, A. Miyamoto and M. Koyama, *Angew. Chem.*, 2010, **122**, 5476-5479.
13. J. Yang, F. Zhao and B. Zeng, *RSC Advances*, 2015, **5**, 22060-22065.
14. M. B. Solomon, T. L. Church and D. M. D'Alessandro, *CrystEngComm*, 2017, **19**, 4049-4065.
15. C.-W. Kung, T. C. Wang, J. E. Mondloch, D. Fairen-Jimenez, D. M. Gardner, W. Bury, J. M. Klingsporn, J. C. Barnes, R. Van Duyne, J. F. Stoddart, M. R. Wasielewski, O. K. Farha and J. T. Hupp, *Chem. Mater.*, 2013, **25**, 5012-5017.
16. C. R. Wade, M. Li and M. Dincă, *Angew. Chem. Int. Ed.*, 2013, **52**, 13377-13381.

17. T. L. Easun, J. Jia, T. J. Reade, X.-Z. Sun, E. S. Davies, A. J. Blake, M. W. George and N. R. Champness, *Chem. Sci.*, 2014, **5**, 539-544.
18. T. L. Easun, J. Jia, J. A. Calladine, D. L. Blackmore, C. S. Stapleton, K. Q. Vuong, N. R. Champness and M. W. George, *Inorg. Chem.*, 2014, **53**, 2606-2612.
19. A. J. Blake, N. R. Champness, T. L. Easun, D. R. Allan, H. Nowell, M. W. George, J. Jia and X.-Z. Sun, *Nat. Chem.*, 2010, **2**, 688-694.
20. S. Castellanos, F. Kapteijn and J. Gascon, *CrystEngComm*, 2016, **18**, 4006-4012.
21. C. L. Jones, A. J. Tansell and T. L. Easun, *J. Mater. Chem. A*, 2016, **4**, 6714-6723.
22. F.-X. Coudert, *Chem. Mater.*, 2015, **27**, 1905-1916.
23. J. Szanyi, M. Daturi, G. Clet, D. R. Baer and C. H. F. Peden, *Phys. Chem. Chem. Phys.*, 2012, **14**, 4383-4390.
24. R. Hinogami, S. Yotsuhashi, M. Deguchi, Y. Zenitani, H. Hashiba and Y. Yamada, *ECS Electrochem. Lett.*, 2012, **1**, H17-H19.
25. D. M. D'Alessandro, *Chem. Commun.*, 2016, **52**, 8957-8971.
26. P. M. Usov, C. Fabian and D. M. D'Alessandro, *Chem. Commun.*, 2012, **48**, 3945-3947.
27. D. Zacher, O. Shekhah, C. Woll and R. A. Fischer, *Chem. Soc. Rev.*, 2009, **38**, 1418-1429.
28. M. Meilikhov, S. Furukawa, K. Hirai, R. A. Fischer and S. Kitagawa, *Angew. Chem. Int. Ed.*, 2013, **52**, 341-345.
29. M. C. So, S. Jin, H.-J. Son, G. P. Wiederrecht, O. K. Farha and J. T. Hupp, *J. Am. Chem. Soc.*, 2013, **135**, 15698-15701.
30. A. Summerfield, I. Cebula, M. Schröder and P. H. Beton, *J. Phys. Chem. C*, 2015, **119**, 23544-23551.
31. Y. Yan, S. Yang, A. J. Blake and M. Schröder, *Acc. Chem. Res.*, 2014, **47**, 296-307.
32. B. Gole, A. K. Bar, A. Mallick, R. Banerjee and P. S. Mukherjee, *Chem. Commun.*, 2013, **49**, 7439-7441.
33. F. Moreau, D. I. Kolkolov, A. G. Stepanov, T. L. Easun, A. Dailly, W. Lewis, A. J. Blake H. Nowell, M. Lenos, E. Besley, S. Yang and M. Schroder, *Proc. Nat. Acad. Sci.*, 2017, **114**, 3056-3061
34. Z. Wei, W. Lu, H.-L. Jiang and H.-C. Zhou, *Inorg. Chem.*, 2013, **52**, 1164-1166.
35. A. Laforgue, T. Addou and D. Bélanger, *Langmuir*, 2005, **21**, 6855-6865.
36. E. Biemmi, C. Scherb and T. Bein, *J. Am. Chem. Soc.*, 2007, **129**, 8054-8055.
37. O. Shekhah, H. Wang, S. Kowarik, F. Schreiber, M. Paulus, M. Tolan, C. Sternemann, F. Evers, D. Zacher, R. A. Fischer and C. Wöll, *J. Am. Chem. Soc.*, 2007, **129**, 15118-15119.
38. C. Munuera, O. Shekhah, H. Wang, C. Woll and C. Ocal, *Phys. Chem. Chem. Phys.*, 2008, **10**, 7257-7261.
39. H. K. Arslan, O. Shekhah, J. Wohlgemuth, M. Franzreb, R. A. Fischer and C. Wöll, *Adv. Funct. Mater.*, 2011, **21**, 4228-4231.

40. A. J. Bard and L. R. Faulkner, *Electrochemical Methods: Fundamentals and Applications*, Wiley VCH, 2nd edn., 2001.
41. A. Paine and R. Loutfy, *Re.s Chem. Intermed.*, 1984, **5**, 227-248.
42. N. G. Connelly and W. E. Geiger, *Chem. Rev.*, 1996, **96**, 877-910.
43. Y. Inokuma, M. Kawano and M. Fujita, *Nat. Chem.*, 2011, **3**, 349-358.
44. C. S. Diercks, Y. Liu, K. E. Cordova and O. M. Yaghi, *Nat. Mater.*, 2018, **17**, 301-307.
45. S. Creager, C. J. Yu, C. Bamdad, S. O'Connor, T. MacLean, E. Lam, Y. Chong, G. T. Olsen, J. Luo, M. Gozin and J. F. Kayyem, *J. Am. Chem. Soc.*, 1999, **121**, 1059-1064.

Figures and Legends

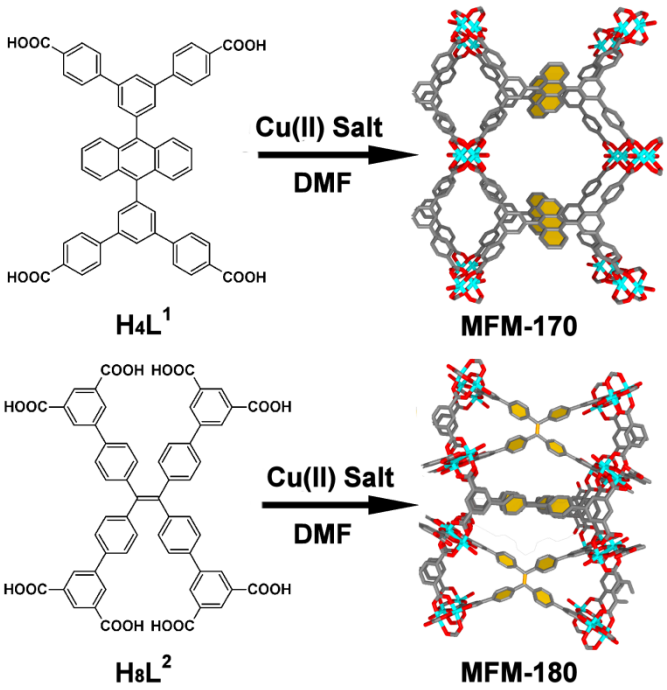

Figure 1: Synthesis and structure of MFM-170 (top) and MFM-180 (bottom). The redox-active core of these two MOFs are highlighted in yellow. Colour code: C: Dark gray, Cu: Blue, O: Red.

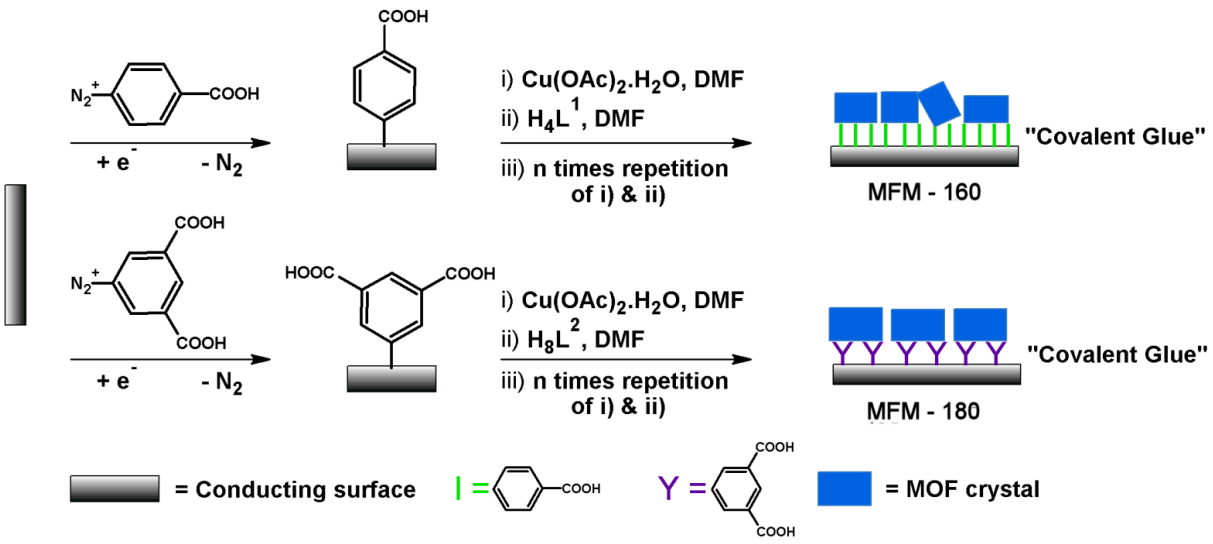

Figure 2: Illustration of chemical modification of conducting surface with crystalline MOF films.

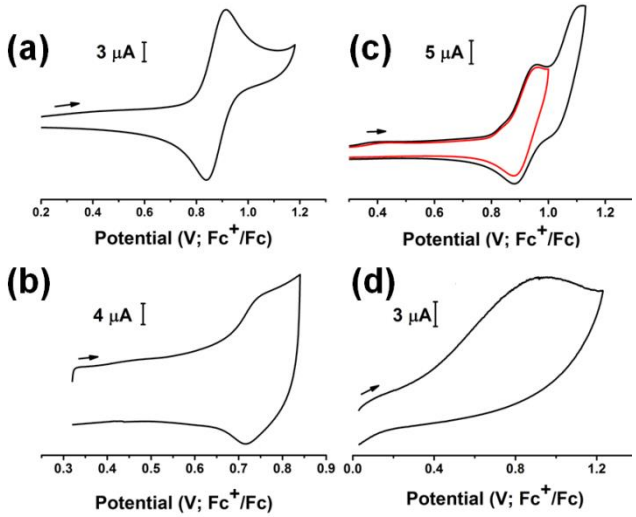

Figure 3: Cyclic voltammograms of (a) $[Et_4L^1]$, (b) thin film of MFM-170, (c) $[Et_8L^2]$ and (d) thin film of MFM-180, recorded at ambient temp in 0.4 M $[(^nBu)_4N]BF_4$ solution in CH_2Cl_2.

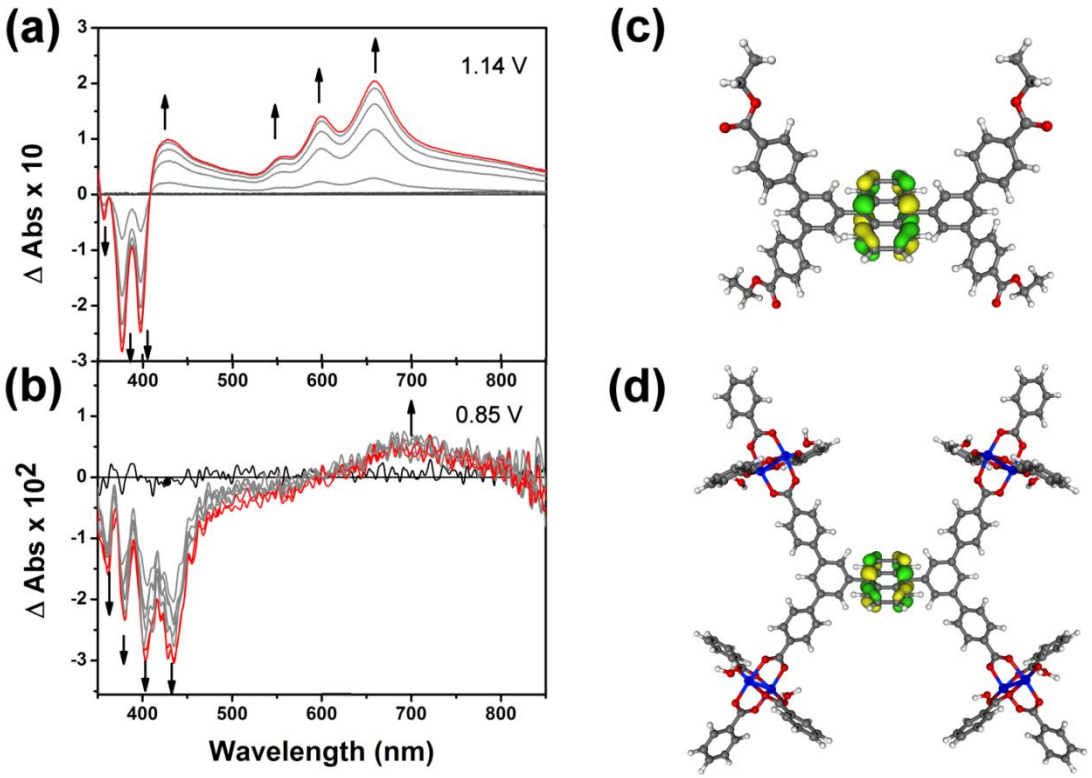

Figure 4: Time-dependent difference spectra of electrochemically oxidised (a) Et_4L^1 and (b) thin film of MFM-170. Spectral noise observed here is the result of low quantity of MFM-170 and discontinuous nature of the MOF film. Potentials are reported *vs* Fc^+/Fc. Kohn-Sham frontier orbital (HOMO) of (c) Et_4L^1 and (d) model system for MFM-170. Colour code: C: dark grey, H: light grey, Cu: blue, O: red, HOMO: green and yellow.

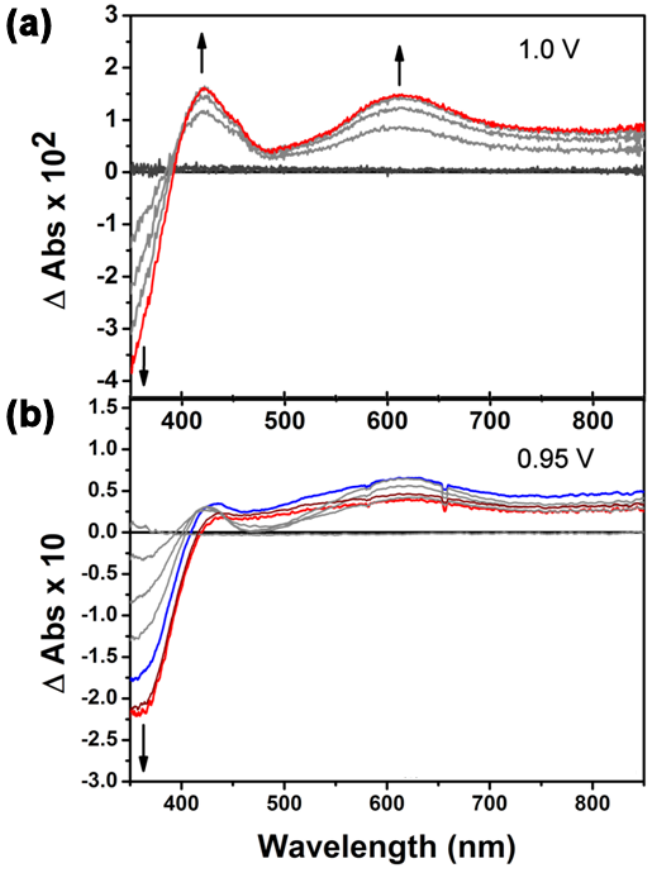

Figure 5: Time-dependent difference spectra of electrochemically oxidised (a) Et_8L^2 and (b) thin film of MFM-180. Potentials are reported *vs* Fc^+/Fc. The blue trace in (b) indicates the point when concentration of the oxidised species $[MFM\text{-}180]^{\bullet+}$ is highest (~8min), while the red trace indicates the final concentration after ~ 15 min.

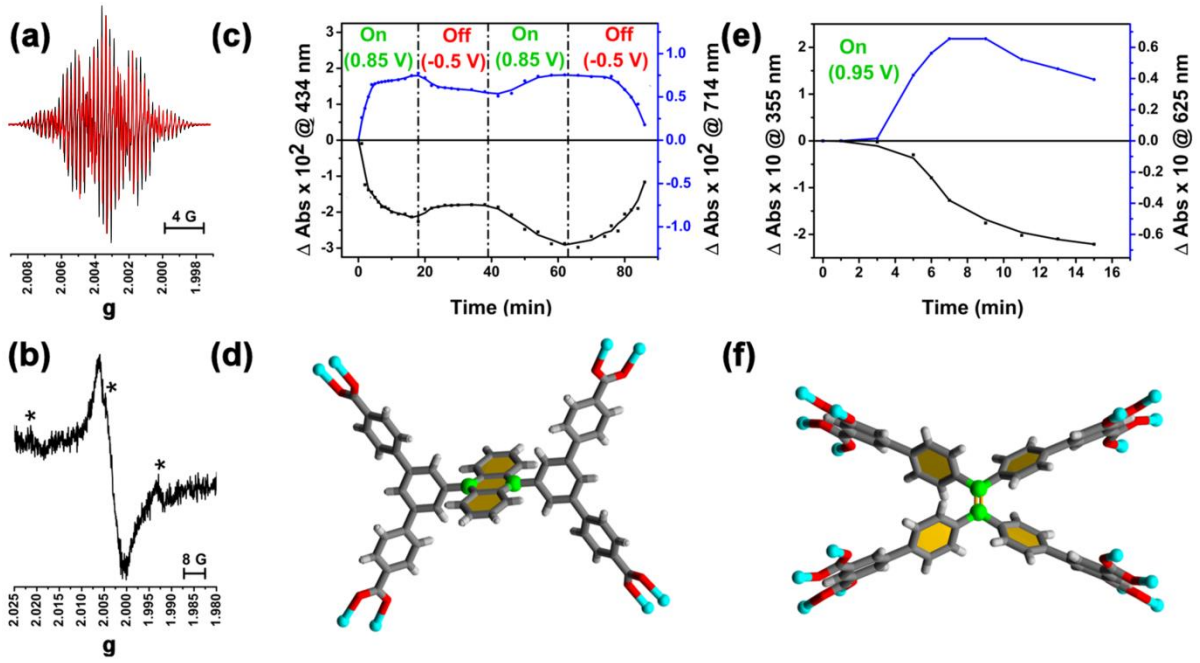

Figure 6: EPR spectra of (a) oxidised Et_4L^1 (black trace: experimental, red trace: simulated) and (b) oxidized film of MFM-170. The mark '*' denotes a possible impurity from NO from the reduction of $NOBF_4$. The time-dependent changes in UV-Vis absorbance for (c) thin film of MFM-170 and (e) thin film of MFM-180 recorded as a response towards electrochemical oxidation at ambient temperature at specific potentials. Black traces in both cases indicates, π–π* transitions of neutral species whereas blue traces show changes in π–π* transitions of oxidized species. Also shown co-ordinating environment of the ligand (d) $[Et_4L^1]^{4-}$ and (f) $[Et_8L^2]^{8-}$. Two carbon atoms for a possible site of the nucleophilic attack have been highlighted in green. Colour code: C: dark grey, H: light grey, Cu: blue, O: red. Note; in case of (d) two carbon atoms for nucleophilic attack are more sterically crowded.

Graphic for Table of Contents

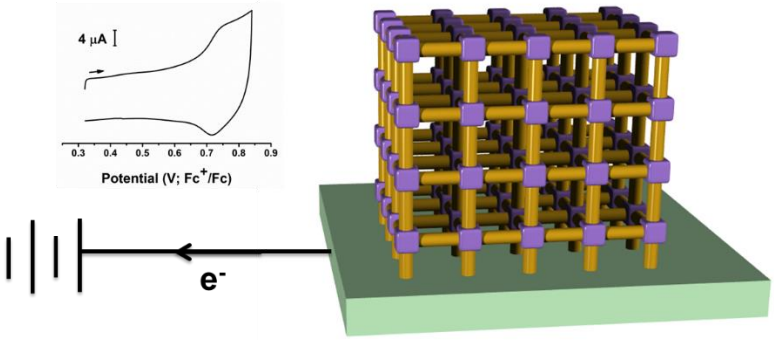

Two different SURMOF films have been grown on conducting surfaces. The SURMOF films on a transparent conducting surface were used for spectro-electrochemical characterisation of radical species.

Supporting Information

Characterisation of Redox States of Metal-Organic Frameworks by Growth on Modified Thin-film Electrodes

Tamoghna Mitra,[a,b] Florian Moreau,[a,c] Adam Nevin,[a,c] Carlo U. Perotto,[a] Alex Summerfield,[d] E. Stephen Davies,[a] Elizabeth A. Gibson,[a,e] Timothy L. Easun,[a,f,]* and Martin Schröder[a,b]*

g. School of Chemistry, The University of Nottingham, University Park Nottingham, NG7 2RD, UK

h. Department of Chemistry, The University of Liverpool, Crown Street, Liverpool, L69 7ZD, UK

i. School of Chemistry, The University of Manchester, Oxford Road, Manchester M13 9PL, UK

j. School of Physics and Astronomy, The University of Nottingham, University Park Nottingham, NG7 2RD, UK

k. School of Chemistry, Bedson Building, Newcastle University, Newcastle upon Tyne NE1 7RU, UK

l. School of Chemistry, Cardiff University, Park Place, Cardiff, CF10 3AT, UK

Experimental Section

Instrumentation. Electrochemical measurements were made using an Eco Chemie Autolab PGSTAT20 potentiostat. All solutions were purged with a stream of Ar prior to use. Cyclic voltammograms were performed using a three-electrode system, with a Pt wire secondary electrode and a saturated calomel reference electrode. For solution based cyclic voltammetry a glassy carbon working electrode was used, and before each measurement, the electrode was cleaned using a polishing pad. All potentials are referenced to the Fc^+/Fc couple used as an internal standard. Cyclic voltammograms were recorded for solutions of compound (*ca.* 1 mM) in the presence of $[N^nBu]_4[BF_4]$ (0.4 M) as supporting electrolyte. Coulometric measurements were performed in an H-cell at 273 K in CH_2Cl_2 containing $[N^nBu_4][BF_4]$ (0.4 M); the cell consisted of a Pt/Rh gauze basket working electrode separated by a glass frit from a Pt/Rh gauze secondary electrode. A saturated calomel reference electrode was bridged to the test solution through a vycor frit oriented at the centre of the working electrode, and the solution was stirred rapidly during electrolysis using a magnetic stirrer bar.

UV-visible spectroelectrochemical measurement on Et_4L^1 and Et_8L^2 were carried out using an optically transparent electrode mounted in a modified quartz cuvette with an optical path length of 0.5 mm. A three-electrode configuration consisting a Pt/Rh gauze working electrode, a Pt wire secondary electrode (in a fritted PTFE sleeve) and a saturated calomel electrode, chemically isolated from the test solution *via* a bridge containing electrolyte solution and terminated in a porous frit, was used in the cell. The potential at the working electrode was controlled by a Sycopel Scientific Ltd DD10M potentiostat. The UV-visible spectra were recorded on a Perkin Elmer Lambda 16 spectrophotometer. The spectrometer cavity was purged with N_2 and temperature control at the sample was achieved by flowing cooled N_2 across the surface of the cell. UV-visible spectroelectrochemical experiments on thin films of MOFs were carried out by using an Ocean Optics Jaz spectrometer equipped with tungsten and deuterium light sources. X-band EPR spectra were recorded on a Bruker EMX spectrometer. The simulations of the EPR spectra were performed using the Bruker

WINEPR SimFonia package Powder X-ray diffraction patterns were collected on a Panalytical diffractometer using Cu-Kα radiation (λ = 1.5418 Å) in reflection mode.

AFM measurements were recorded on films grown on the ITO surface by loading the MOF-modified-substrate into an Asylum Research Cypher-S AFM. AFM images were obtained in repulsive amplitude modulated (AC mode) using Olympus AC240-TS AFM cantilevers (Asylum research). AFM images were processed using the Gwyddion software package.

Unless otherwise stated, reagents were used as received from the suppliers (Sigma-Aldrich, Acros Organic and Fluka) and all reactions, manipulations and transfers were performed under an inert atmosphere of Ar using standard Schlenk techniques. For electrochemical analysis, solvents were dried and degassed following standard procedures and stored under Ar in Young's ampoules over molecular sieves (pore size 4 Å). High-purity Ar was obtained from BOC gases and used without any further purification. Indium doped tin oxide glass (150 nm coating, 12 ohms per square) was obtained from Visiontek Glass and cleaned by washing and sonicating in acetonitrile. Conducting carbon paper was obtained from SGL and was cleaned in a similar way before use.

H_8L^2, Et_8L^2 (H_8L^2 = 4',4''',4'''''',4''''''''-(ethene-1,1,2,2-tetrayl)tetrakis(([1,1'-biphenyl]-3,5-dicarboxylic acid) and Et_8L^2 = octaethyl 4',4''',4'''''',4''''''''-(ethene-1,1,2,2-tetrayl)tetrakis([1,1'-biphenyl]-3,5-dicarboxylate)) were synthesized as reported previously.[S1] H_4L^1 and Et_4L^1 (H_4L^1 = 5', 5''''-(anthracene-9,10-diyl)bis(([1,1':3',1''-terphenyl]-4,4''-dicarboxylic acid)), Et_4L^1 = tetraethyl 5',5''''-(anthracene-9,10-diyl)bis([1,1':3',1''-terphenyl]-4,4''-dicarboxylate) were synthesized as follows.

Scheme S1: Synthesis of Et_4L^1 and H_4L^1

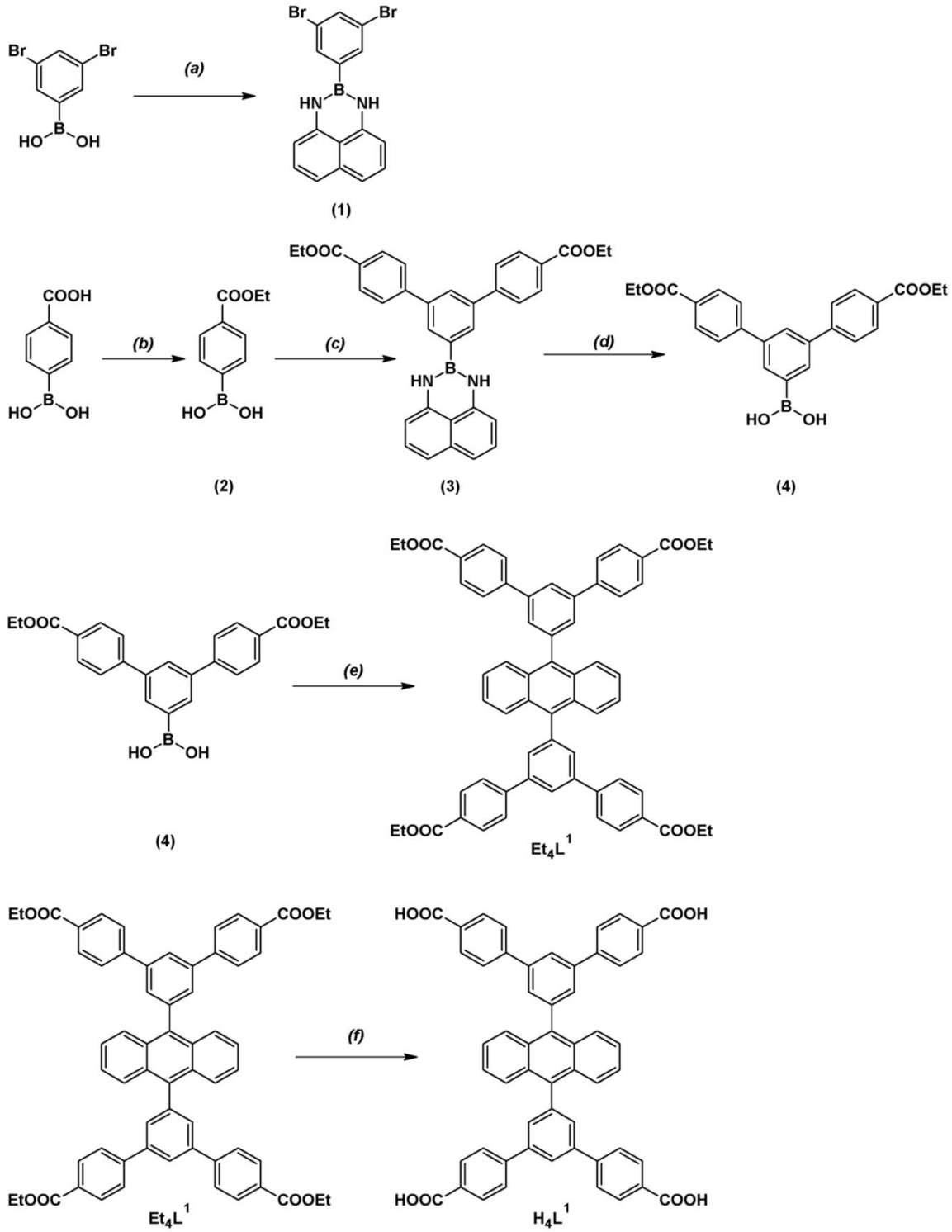

(a) : 1,8-diaminonapthalene, toluene, 100 °C 1 h
(b) : Ethanol, Conc. Sulphuric acid, reflux 19 h
(c) : (i) (1), Potassium Carbonate, Toluene/water 60 °C, Ar
(ii) Tri-^{t}butyl phosphine, tris(dibenzylideneacetone)dipalladium(0), 80 °C 90 min, Ar
(d) : THF, 2M sulphuric acid, reflux 4 h
(e) : (i) 9,10 dibromo anthracene, Potassium Carbonate, Toluene/water 60 °C, Ar
(ii) Tri-tbutyl phosphine, tris(dibenzylideneacetone)dipalladium(0), 80 °C 150 min, Ar
(f) : (i) THF/EtOH, 2M NaOH(aq), reflux, 23 h; (ii) HCl(aq)

Synthesis of Et_4L^1 and H_4L^1

Synthesis of 2-(3,5-dibromophenyl)-2,3-dihydro-1H-naphtho[1,8-de][1,3,2]diaza borinine, 1.

To a stirred solution of (3,5-dibromophenyl) boronic acid (10.0 g, 36 mmol) in toluene (170 mL) was added 1,8-diaminonapthalene (6.6 g, 42 mmol). The solution was heated to 100 ^oC for 1 h and the solvent removed under reduced pressure to give the crude product as a brown solid. The solid was dissolved in a minimum volume of boiling CH_2Cl_2, and the crude product precipitated by addition of petroleum ether (b.p 60-80 °C). The suspension was allowed to cool to room temperature, and the solid was separated by filtration and dried (80 °C) to obtain pure product as a bright yellow solid (11.3 g, 78%). Spectroscopic analysis and purity of the compound were in accordance to those found in literature.[S2]

Synthesis of 4-ethoxycarbonylphenyl boronic acid, 2

To a stirred solution of 4-carboxyphenylboronic acid (15.0 g, 90 mmol) in EtOH (375 mL) was added concentrated H_2SO_4 (4.5 mL). The solution was heated at reflux for 19 h and the solution concentrated under reduced pressure until a precipitate formed. An excess of water was added to the suspension, which was collected by filtration. The solid product was washed with water until the filtrate was pH 7, and then dried (80 °C) to give the product as a fine white powder (15.4 g, 88%).

Synthesis of 5'-(1H-naphtho[1,8-de][1,3,2]diazaborinin-2(3H)-yl)-[1,1':3',1''-terphenyl]-4,4''-dicarboxylate diethyl ester, 3

To a stirring, degassed suspension of **1** (6.0 g, 15 mmol), **2** (8.13 g, 41 mmol) and K_2CO_3 (4.34 g, 44 mmol) in toluene (400 mL) and water (100 mL) at 60 °C was added tri-tert-butyl phosphine (1M in toluene, 2.4 mL, 2.4 mmol) and tris(dibenzylideneacetone)dipalladium(0) (1.34 g, 1.5 mmol). The reaction mixture was heated to 80 °C for 1.5 hours, and the resulting suspension filtered while hot. The solid was extracted with CH_2Cl_2 (200 mL) and

the organic phase washed with water (2 x 200 mL), dried over $MgSO_4$ and filtered. The solvent was removed under reduced pressure and the resulting black oil was dissolved in a minimum volume of CH_2Cl_2 and the solution passed through a silica plug using ethyl acetate as eluent. The filtrate was evaporated to dryness under reduced pressure to give a dark brown solid. The solid was dissolved in a minimum volume of boiling CH_2Cl_2, and precipitated by addition of petroleum ether (b.p. 60-80 ^oC). The product was separated by filtration and dried (80 °C) to obtain the pure product as a yellow/orange solid (5.98 g, 74%). (Found: [M], 540.13. $C_{34}H_{29}O_4N_2B$ requires 540.22); ^1H NMR (300MHz, $CDCl_3$): δ = 1.46 (t, $^3J_{H,H}$ 7.1 Hz, 6H, CH_3), 4.45 (q, $^3J_{H,H}$ 7.1 Hz, 4H, CH_2), 6.15 (s, 2H, NH), 6.49 (d $^3J_{H,H}$ 7.1 Hz, 2H, Ar), 7.10-7.22 (m, 4H, Ar), 7.78 (dt, $^3J_{H,H}$ 8.5 Hz, $^3J_{H,H}$ 1.9 Hz, 4H, Ar), 7.90 (d, $^3J_{H,H}$ 1.8 Hz, 2H, Ar), 7.94 (t, $^3J_{H,H}$ 1.8 Hz, 1H, Ar), 8.20 (dt, $^3J_{H,H}$ 8.5 Hz, $^3J_{H,H}$ 1.9 Hz, 4H, Ar) ppm. ^{13}C NMR (100 MHz, $CDCl_3$): δ = 14.42, 61.06, 106.19, 118.22, 127.30, 127.63, 127.69, 128.19, 129.75, 130.14, 130.24, 140.82, 140.89, 145.17, 166.44 ppm.

Synthesis of 4,4''-bis(ethoxycarbonyl)-[1,1':3',1''-terphenyl]-5'-yl)boronic acid, 4

To a stirred solution of **3** (6.35 g, 11.8 mmol) in tetrahydrofuran (360 mL) was added H_2SO_4 (2M, 73 mL) and the solution heated under reflux for 4 h. The reaction mixture formed a suspension over this time, and this was filtered while hot to remove the solid impurities. The filtrate was reduced under reduced pressure until a precipitate formed. This suspension was re-solubilised by heating to 70 °C, and an excess of water was added to precipitate a solid. The mixture was filtered and the solid collected and washed with a large volume of water until the filtrate was at pH = 7. The product was dried (80 °C) to give an off white solid (4.44 g, 97%). (Found: [M - H], 417.1585. $C_{24}H_{22}O_6B^-$ requires 417.1509); ^1H NMR (300MHz, $CDCl_3$): δ = 1.36 (t, $^3J_{H,H}$ 7.1 Hz, 6H, CH_3), 4.36 (q, $^3J_{H,H}$ 7.1 Hz, 4H, CH_2), 7.96 (d $^3J_{H,H}$ 8.3 Hz, 4H, Ar), 8.08 (d, $^3J_{H,H}$ 8.3 Hz, 5H, Ar), 8.21 (d, $^3J_{H,H}$ 1.8 Hz,

2H, Ar) ppm. ^{13}C NMR (100 MHz, CDCl3): δ = 14.67, 61.33, 86.17, 92.38, 127.62, 128.43, 129.23, 130.23, 139.24, 145.25, 166.08 ppm.

Synthesis of Et_4L^1 (tetraethyl 5',5''''-(anthracene-9,10-diyl)bis([1,1':3',1''-terphenyl]-4,4''-dicarboxylate)

To a stirring, degassed solution of 9,10-dibromoanthracene (474 mg, 1.41 mmol), **4** (1.65 g, 4.2 mmol) and K_2CO_3 (1.09 g, 11 mmol) in toluene (133 mL) and water (34 mL) at 60 °C was added tri-tert-butyl phosphine (1M in toluene, 0.65 mL, 0.65 mmol) and tris(dibenzylideneacetone)dipalladium(0) (258 mg, 0.28 mmol). This suspension was heated at 80 °C for 2.5 hours. The workup procedure was the same as for **3**. The product was a yellow solid (1.06 g, 82%). (Found: [M], 922.21. $C_{62}H_{50}O_8$ requires 922.35); ^{1}H NMR (300MHz, $CDCl_3$): δ = 1.45 (t, $^3J_{H,H}$ 7.2 Hz, 12H, CH_3), 4.44 (q, $^3J_{H,H}$ 7.2 Hz, 8H, CH_2), 7.40-7.47 (m, 4H, Ar), 7.80-7.90 (m, 16H, Ar) 8.10 (t, $^3J_{H,H}$ 1.7 Hz, 2H, Ar), 8.18 (dt, $^3J_{H,H}$ 8.5 Hz, $^3J_{H,H}$ 1.9 Hz, 8H, Ar) ppm. ^{13}C NMR (100 MHz, CDCl3): δ = 14.47, 61.13, 86.17, 108.20, 125.62, 127.22, 130.23, 131.43, 139.44, 141.01, 141.04, 149.25, 156.86, 171.28, 171.48 ppm.

Synthesis of H_4L^1 5',5''''-(anthracene-9,10-diyl)bis([1,1':3',1''-terphenyl]-4,4''-dicarboxylic acid).

To a stirred solution of Et_4L^1 (1.00 g, 1.1 mmol) in tetrahydrofuran (140 mL) and EtOH (140 mL) was added NaOH (2M, 140 mL), and the reaction mixture heated at 100 °C for 23 h. The cooled solution was filtered, and the filtrate was observed to have two phases. The aqueous phase was separated, acidified with HCl (pH ~1), and the resulting suspension was filtered and the solid collected and washed with water until the filtrate was at pH = 7. The product was then dried (80 °C) to give a brown solid (874 mg, 99%). (Found: [M], 810.06. $C_{54}H_{34}O_8$ requires 810.23); ^{1}H NMR (300MHz, $CDCl_3$): δ = 7.43-7.55 (m, 4H, Ar), 7.73-

7.83 (m, 4H, Ar), 7.90 (s, 4H, Ar), 8.06 (s, 16H, Ar), 8.35 (s, 2H, Ar), 13.02 (s, 4H, COOH). ^{13}C NMR (100 MHz, CDCl3): δ = 108.00, 111.40, 123.42, 123.82, 127.82, 128.23, 129.83, 130.43, 139.04, 140.84, 144.05, 156.66 ppm. CHN – Expected: C, 79.99; H, 4.23; O, 15.79, Found: C, 75.8; H, 4.2.

Synthesis of MFM-170 as a solid crystalline powder.

H_4L^1 (10 mg, 0.013mmol) and $Cu(NO_3)_2.2.5H_2O$ (26 mg, 0.11 mmol) were dissolved in DMF (3 mL) and the reaction mixture acidified with aq. HCl (3 drops, 8M). The reaction mixture was heated at 80 ^oC for 16 h in a sealed glass vial (9 mL). After 16 h greenish blue crystals of MFM-170 were collected by filtration, washed with DMF and dried under vacuum. Yield 60%.

Functionalisation of conducting surface.

Indium tin oxide (ITO) coated glasses and carbon paper was treated before each experiment by ultrasonic cleaning in ultrapure H_2O for 15 mins, followed by ultrasonication for 30 min in CH_3CN prior to modification. The diazonium reduction experiment was carried out with 1 mM diazonium salt in a solution of 0.1 M NBu_4ClO_4 in CH_3CN under an inert atmosphere. The modified electrodes were washed with CH_3CN and then ultrasonicated in CH_3CN for 30 min and stored in dry CH_3CN under Ar atmosphere. The barrier properties of the unmodified and the modified electrodes were evaluated in 1 mM ferrocene solution with 0.1M NBu_4ClO_4 in dry CH_3CN.

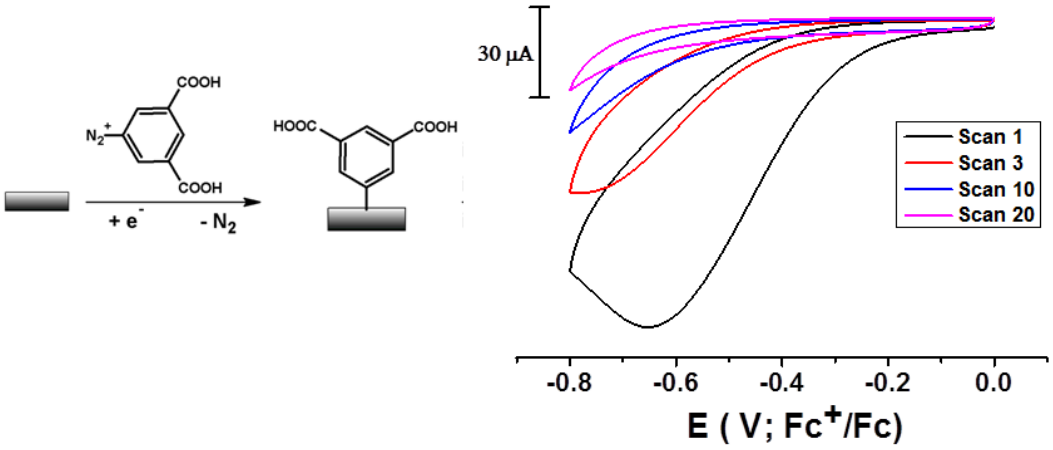

Figure S1: Cyclic voltammograms of an ITO-glass electrode in 1mM diazonium salt in a solution of 0.1 M NBu_4ClO_4 in CH_3CN. Scan rate = 100 mV/s.

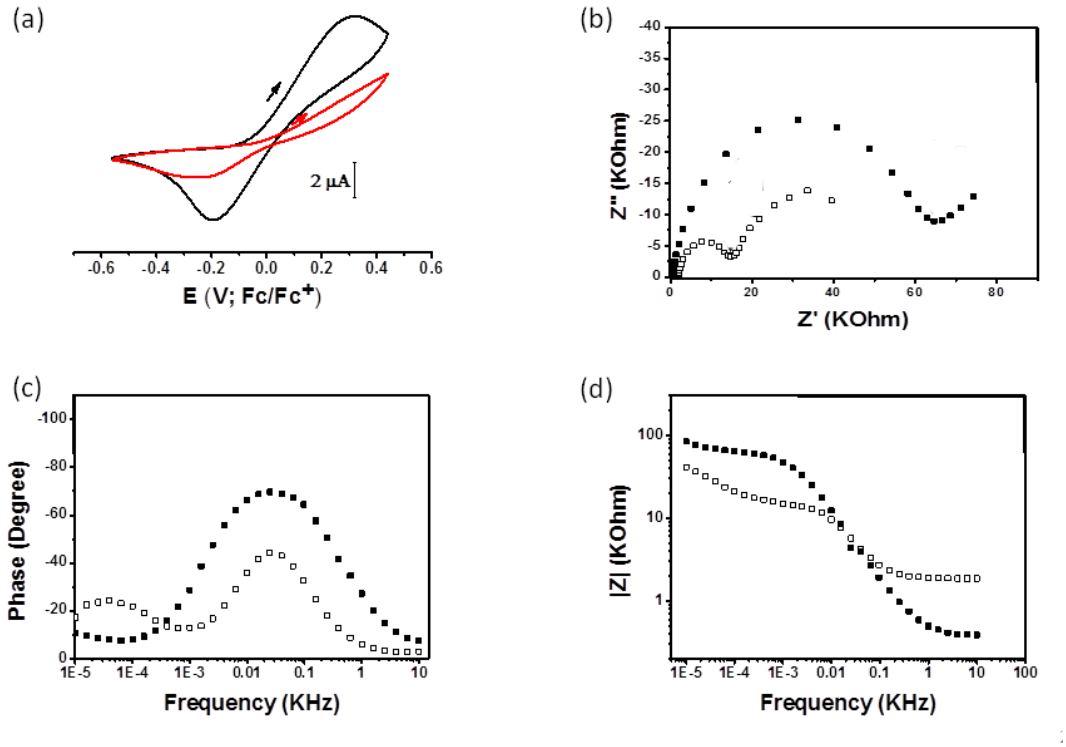

Figure S2: Blocking behaviour of isophthalic acid coated ITO-glass electrode. (a) Cyclic voltammograms of ferrocene solution at a scan rate of 10 mV/s – before (black trace) and after (red trace) coating with isophthalic acid, (b) Nyquist plot and (c-d) Bode plots of ITO glass electrode (open symbol) and isophthalic acid coated electrode (close symbol).

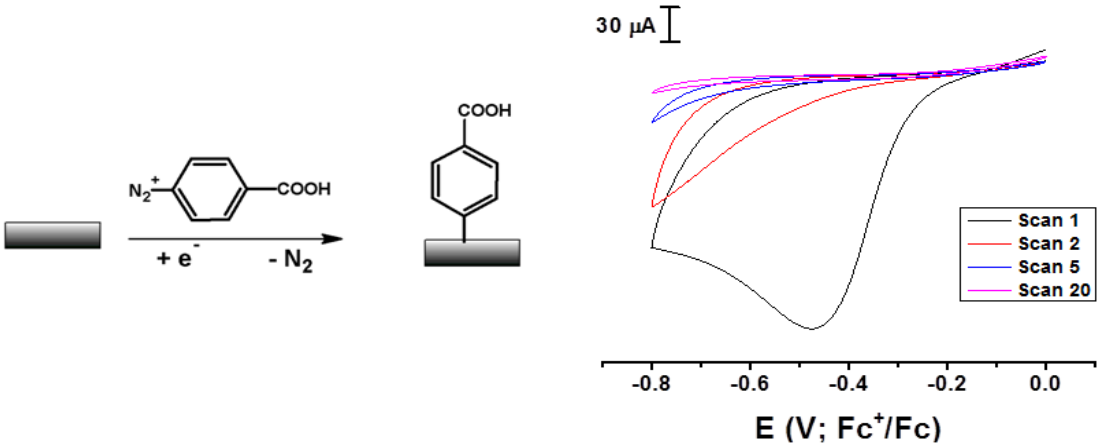

Figure S3: Cyclic voltammograms of an ITO-glass electrode in 1 mM diazonium salt/0.1 M NBu_4ClO_4/CH_3CN solution: Scan rate = 100 mV/s.

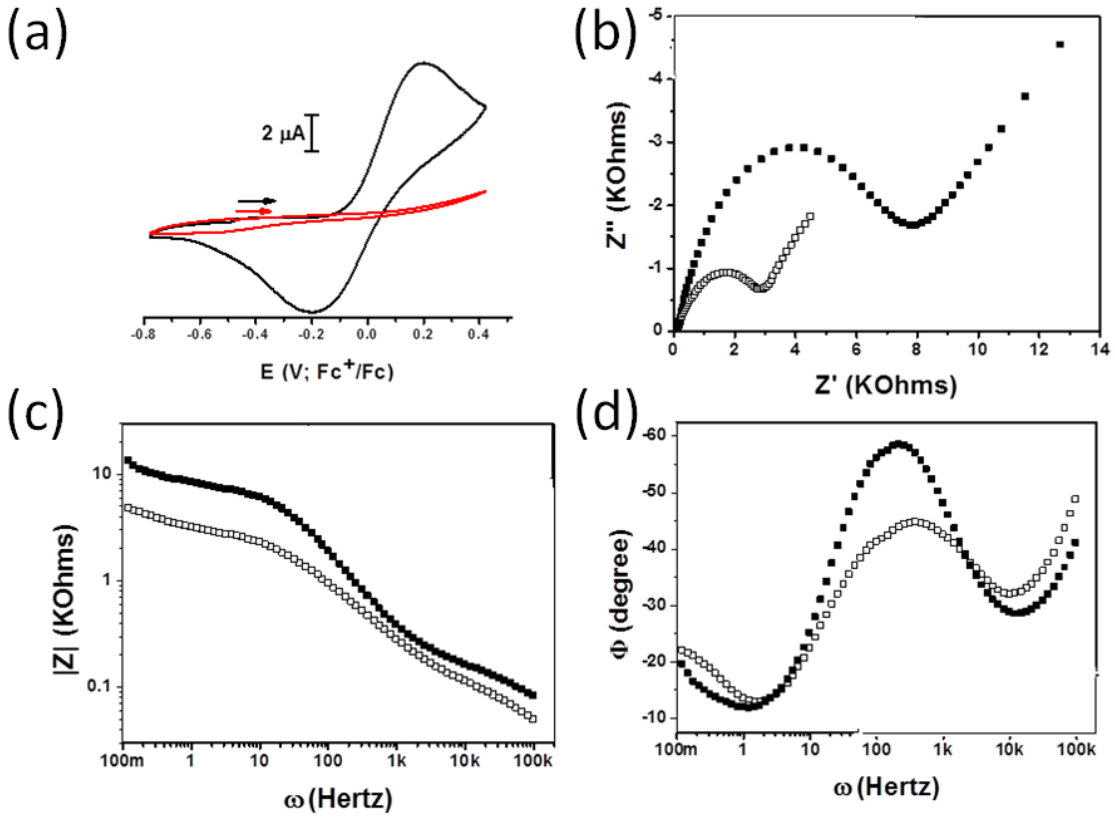

Figure S4: Blocking behaviour of benzoic acid coated ITO-glass electrode. (a) Cyclic voltammograms of ferrocene solution at a scan rate of 10 mV/s – before (black trace) and after (red trace) coating with benzoic acid, (b) Nyquist plot and (c-d) Bode plots of ITO glass electrode (open symbol) and isophthalic acid coated electrode (close symbol).

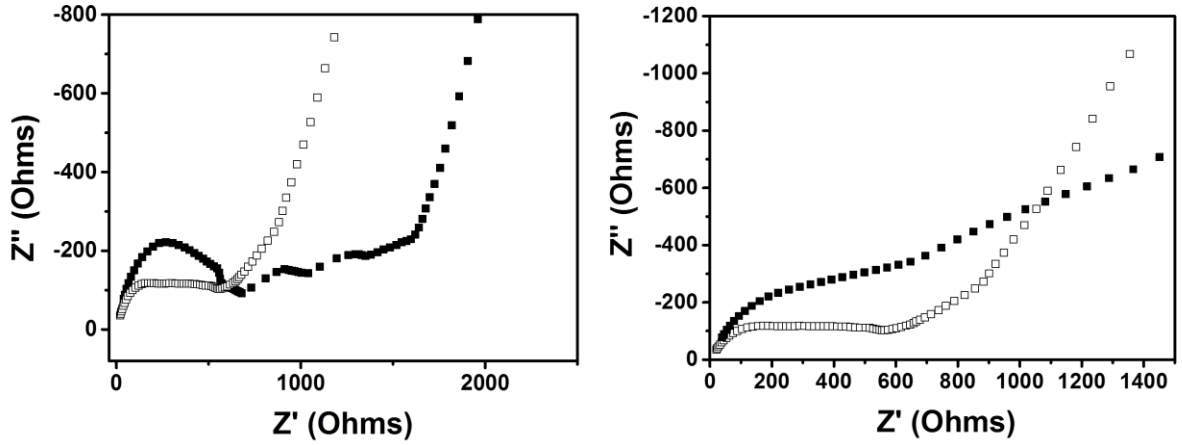

Figure S5: Blocking behaviour of Aryl monolayer coated carbon paper electrode. (~ 1 mm x 1mm): Nyquist plot of (left) isophthalic acid coated C-paper electrode and (right) benzoic acid coated C-paper electrode before and after coating.

Modification of conducting surface with MOF coatings: Separate solutions of ligand (0.2 mM) and $[Cu(OAc)_2].H_2O$ (0.4 mM for MFM-170 film and 0.8 mM for MFM-180) in DMF were freshly prepared for each experiment. Typical experiments were carried out using an in-house-built dip coating system. The conducting surface was immersed sequentially first in $[Cu(OAc)_2].H_2O$ solution and then into the ligand solution for 1 min each. The metal ion solution and ligand solution were not stirred during this process. Between each dipping, the surface was washed by immersion in stirring DMF for 2 min. This whole sequence is considered as one complete cycle. For characterization by PXRD a film with 30 such cycles of dipping was synthesized, while for all electrochemical studies films with 10 such cycles were synthesized. The AFM studies were conducted on films grown by 10 and 20 cycles of sequential dipping.

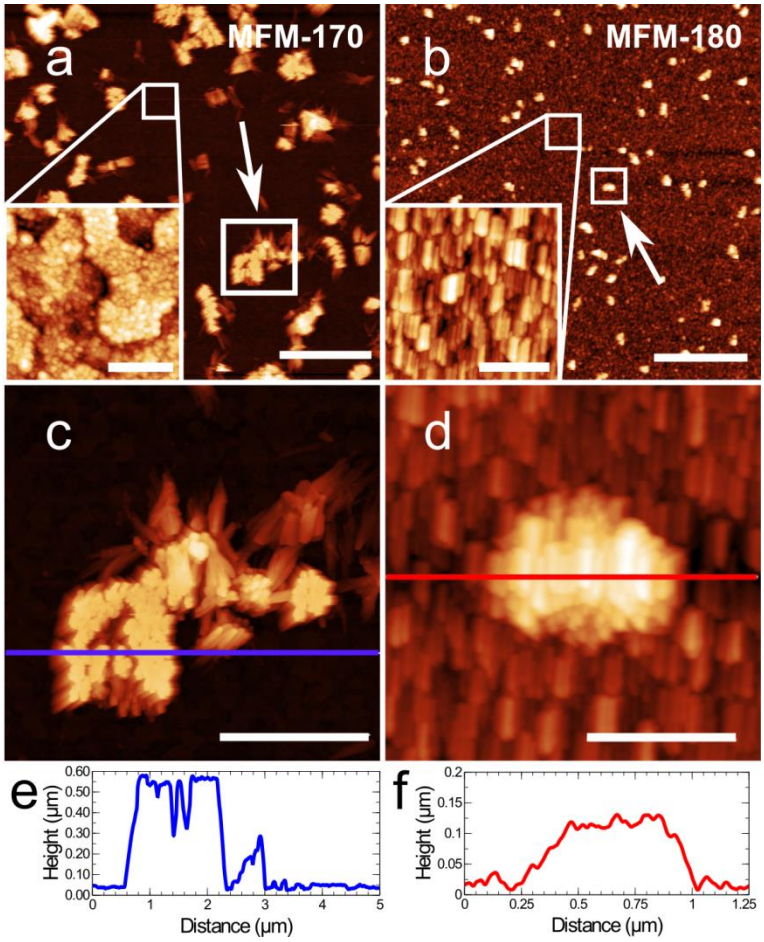

Figure S6: AFM images of (a,c) MFM-170 and (b,d) MFM-180 MOF grown on functionalised ITO substrate after 10 cycles of deposition. Extra crystallites also grow on the surface, apparently not connected to the cyclic deposition. a) AFM image of MFM-170 on ITO, the arrow indicates the region in image c. Scale bar 5 µm. (inset) Image of the region between the agglomerated crystallite deposits of MFM-170, commensurate with blank ITO surface. Scale bar 300 nm. b) AFM image of MFM-180 on ITO, the arrow indicates the region in image d. Scale bar 5 µm. (inset) Image of the region between the agglomerated crystallite deposits of MFM-180, which is also covered by closely packed crystallites of MFM-180, leading to a continuous coverage of MFM-180 on the surface). Scale bar 400 nm. c) High resolution image of the MOF deposit indicated by the arrow in image a. Scale bar 2 µm. d) High resolution image of the region indicated by the arrow in image b. Scale bar 400 nm. e) Height profile along the region marked by the blue line in image c. f) Height profile along the region marked by the red line in image d.

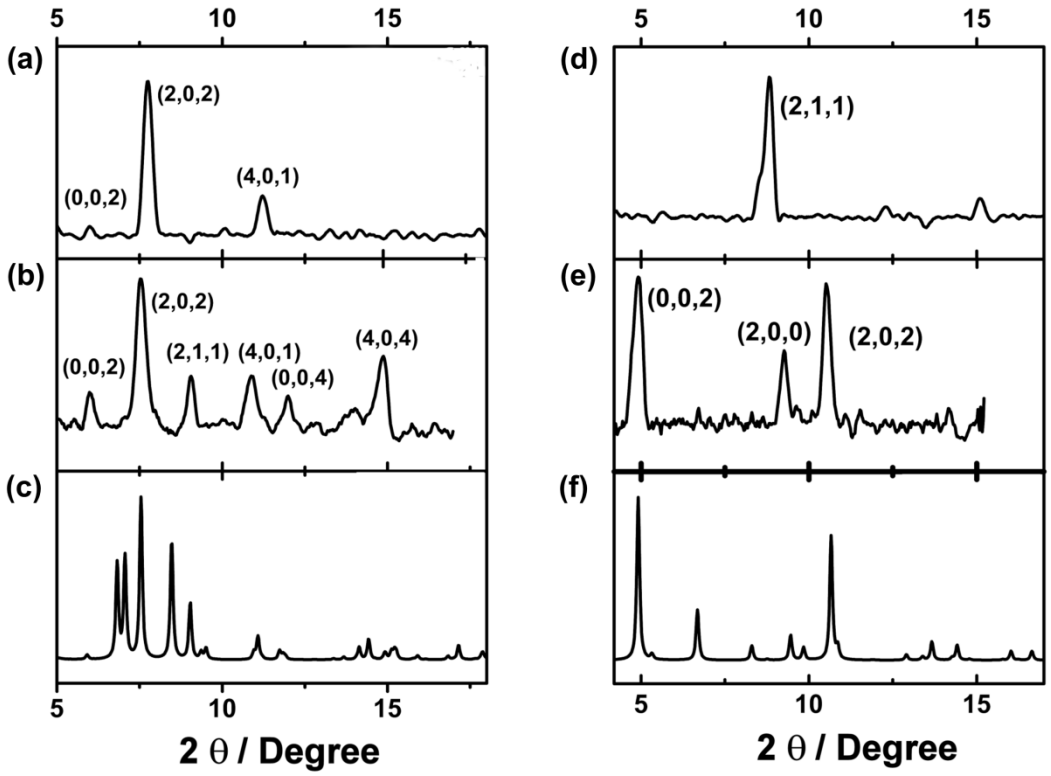

Figure S7: PXRD of **MFM-170** films on (a) ITO electrode, on (b) carbon paper, (c) simulated from single crystal structure, and **MFM-180** films (d) on ITO electrode, on (e) carbon paper, (f) simulated from single crystal structure.

Cyclic Voltammetry (CV) and Bulk Electrolysis of MOF Films.

For all electrochemical studies, MOF films were synthesized from 10 dipping cycles. For cyclic voltammetry, the MOF films grown on carbon paper (1mm x 1mm) were used as working electrodes due to the superior conductivity of carbon paper over an ITO-coated glass. Conversely, the ITO-based films were used as working electrodes for spectroelectrochemical studies to exploit the transparent nature of the ITO-coated glass. Prior to electrochemical experiments the MOF films were immersed in CH_2Cl_2 for 3-4 days, with solvent replaced every 24h. The films were then dried in air and re-immersed in the electrolyte solution of 0.4 M of $[^nBu_4N][BF_4]$ in CH_2Cl_2 for 2-3 days to allow CH_2Cl_2 and

electrolyte to fully exchange with the other guests such as DMF trapped in the MOF pores. This acts as an "electrochemical conditioning" period.

We found that it is necessary to use thinner films (10 cycles of dipping) in order to record the voltammetric response. This can be explained by considering ion transfer through MOF pores. The distance an ion can travel/diffuse during an electrochemical process is usually proportional to $(Dt)^{0.5}$ (where D = diffusion coefficient, t = time).[S3] Therefore it is necessary for films to be thinner than the diffusion layer so that electrolyte can diffuse readily through the pores of the MOF to the electrode surface.

CV Scan Rate (ν) Dependence of Peak Currents (i_p) and Separation (ΔE_p) in MFM-170.

CV measurements of on MFM-170 films on carbon paper were carried out at a series of scan rates (ν = 2, 3, 4, 5, 6, 8, 10 mV/s). The resulting data are plotted in Figure S8. For diffusion limited processes in solution-based measurements, i_p is directly proportional to $\nu^{1/2}$ while ΔEp should be 0.059/n V at 25 ^{o}C. However, for surface-confined processes not subject to diffusion limitation, i_p should be directly proportional to ν and $\Delta E_p = 0$ V. The ΔE_p *vs* scan rate plot (Figure S8) shows that ΔE_p for MFM-170 is not zero, though values are far less than 59mV. To understand the dependence of i_p over scan rate a Ln(i_p) *vs* Ln(scan rate) plot can be used.

$i_p \alpha \nu^n$ where ν = scan rate; $1 \geq n \geq 0.5$

Hence,

$\mathrm{Ln}(i_p) = n\mathrm{Ln}(\nu) + \text{constant}$. [$\mathrm{Ln}(x) = \log_e(x)$]

Therefore, the slope for the data plotted as $\mathrm{Ln}(i_p)$ *vs* Ln(ν) can indicate the order of the dependence with respect to scan rate. For a diffusion limited process, the slope of this plot should approach 0.5, while for a surface confined process the slope should be 1.

For MFM-170 film the slope tends to be closer to 1 for slow scan rates although this deviates from ideal behaviour at the higher scan rate. Such behaviour is not expected from a surface confined species. This phenomenon has been observed in related literature and is explained by taking into account mass transport limitations and slower diffusion of electrolyte through the micro-porous channel.[S3] The MOF modified electrode can be considered as a working electrode, modified by non-conducting crystals having isolated redox active species. However, due to the microporous MOF structure ions can diffuse through the crystals. Hence electrochemical process can be written as:

$MOF + nA^-(sol) - ne^- \rightarrow [\ nA^- \subset (MOF)^{n+}]$

Or

1) $MOF - ne^- \rightarrow (MOF)^{n+}$;
2) $nA^-(sol) + (MOF)^{n+} \rightarrow [\ nA^- \subset (MOF)^{n+}]$

where A- is the counter ion of an electrolyte solution. The sign "⊂" indicates supramolecular assembly involving host and guest (*i.e.* Guest ⊂ Host). If electron transfer is slower compared to diffusion of counter ion A^-, the rate of electron transfer becomes the rate determining step, while the rate of diffusion of A^- will not have any influence on the cyclic voltammogram. A similar situation can be seen at the low scan rate. However, when the rate of diffusion of A^- is slower (or not significantly fast compare to electron transfer), the rate of diffusion of A^- begins to influence the cyclic voltammogram.

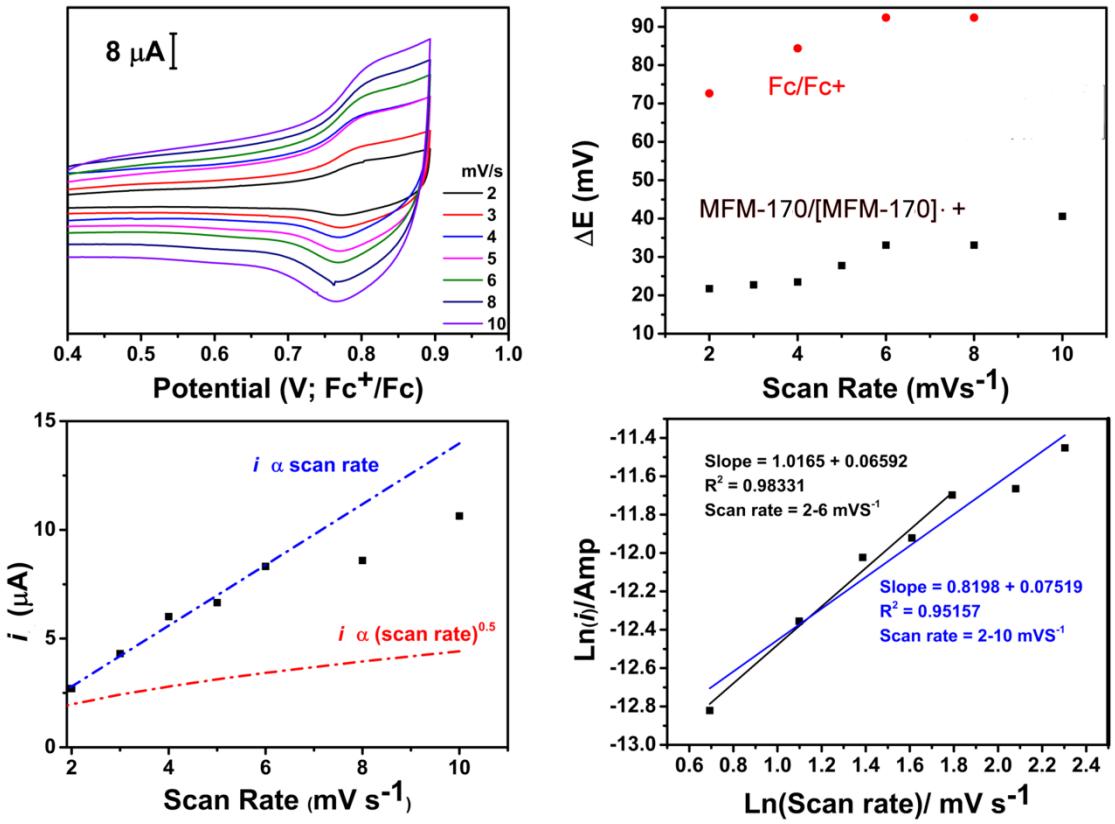

Figure S8: Cyclic voltammetry of MFM-170 film at various scan rates (a) and related analyses (b-d). Dependence of ΔE and i_p on scan rate strongly indicates that the electrochemical oxidation process of MFM-170 is not diffusion limited. This can be further verified by plotting Ln(*i*) *vs* Ln(scan rate); the slope is much higher than 0.5, as would be expected for a classical diffusion limited process. See preceding discussion for details.

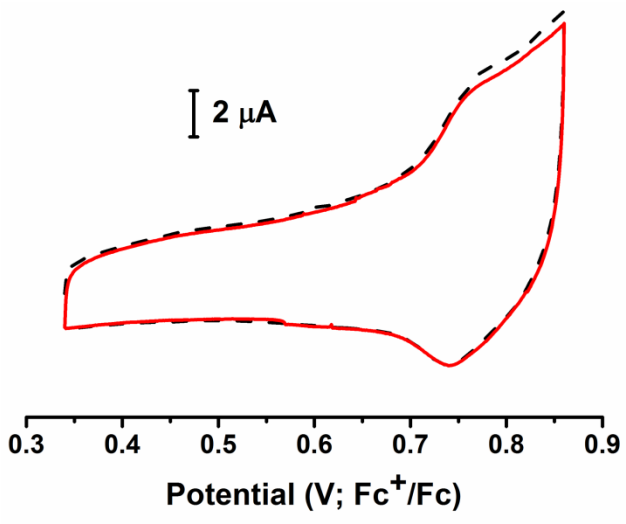

Figure S9: Multiple cycles in the cyclic voltammetric scan for MFM-170 films on carbon paper at scan rate 2 mV s^{-1}. The Broken line represents 1st scan while the solid line represents 3rd scan.

EPR spectroscopy of $[Et_4L^1]^{\bullet+}$

The EPR spectrum of $[Et_4L^1]^{\bullet+}$ can be explained by taking into consideration hyperfine splitting by 3 sets of 4 ^1H (3 x 4 = 12 ^1H). Only the anthracene motif in the ligand has an environment surrounded by 12 ^1H nuclei as shown in Figure S8. Also, the absence of any other hyperfine interactions suggests that the SOMO is confined mainly to the anthracene unit and partially on the adjacent phenyl rings, but not delocalized over the entire molecule.

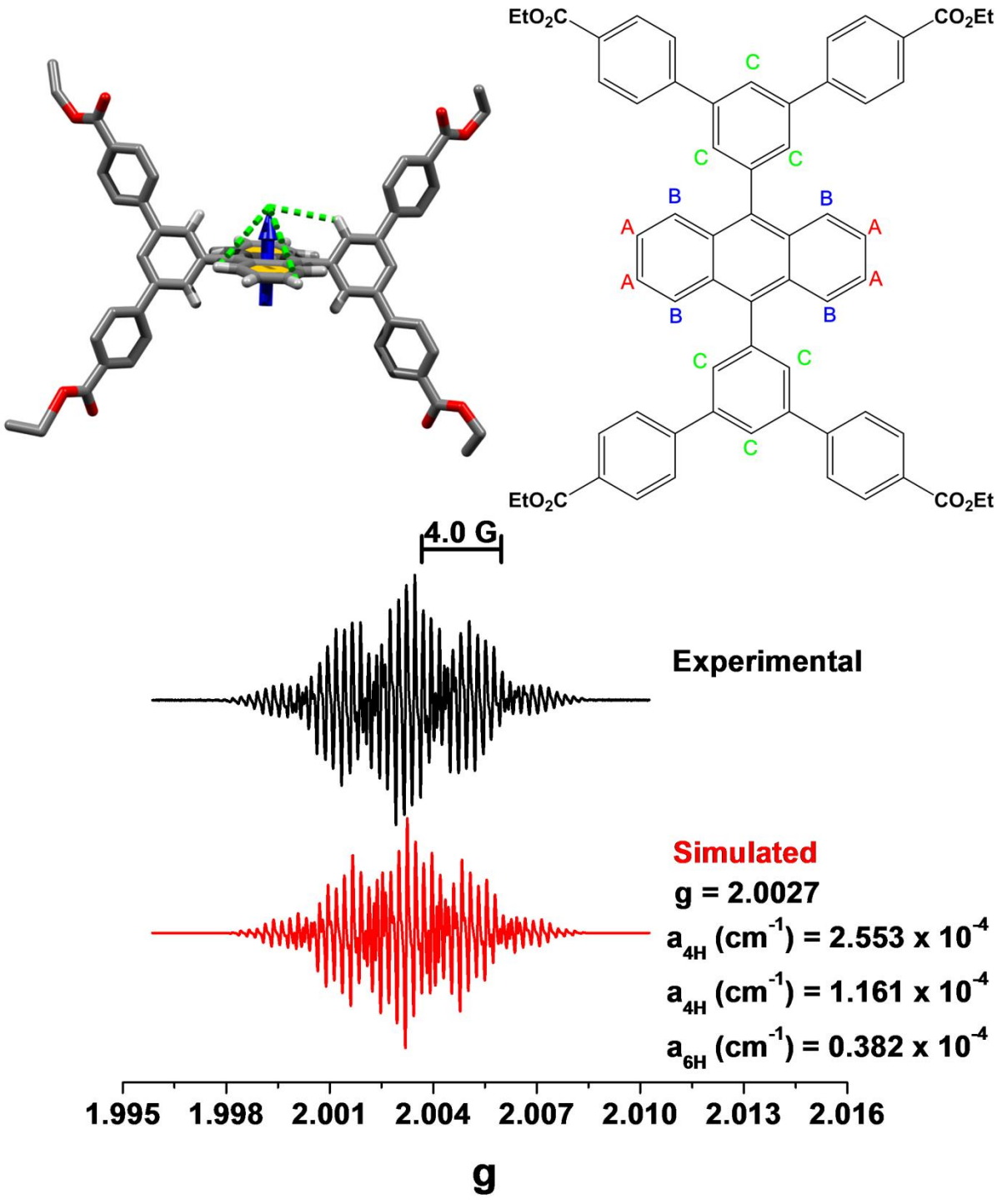

Figure S10: EPR spectrum of $[Et_4L^1]^{\bullet+}$ (bottom). Top: Hyperfine coupling to H centres in the EPR spectrum of $[Et_4L^1]^{\bullet+}$. Colour code: C; black, H; grey, O; red. Blue arrow indicates the position of the radical ion; green lines indicate 3 different hyperfine interactions. Only

protons involved in hyperfine interaction have been shown for simplicity. Three sets of different proton positions are highlighted as ‘A’, ‘B’ & ‘C’

Computational details: All DFT calculations were performed using the program Gaussian 03.[S4] Geometry optimizations were performed using the the Becke three-parameter hybrid exchange functional[S5] and the Lee–Yang–Parr correlation function[S6] (B3LYP) in combination with the the 6-31G(d,p)[S7] basis set for C, H and O atoms and the standard LANL2DZ basis set for the Cu atoms.[S46] After optimization a frequency analysis was performed to confirm that the stationary point was found to be a minimum on the potential energy surface. Molecular models were manipulated using the program Moldraw [S47] and visualization of optimized structure and plot of electronic properties were obtained with the program Molekel (version 5.4.0.8).[S48]

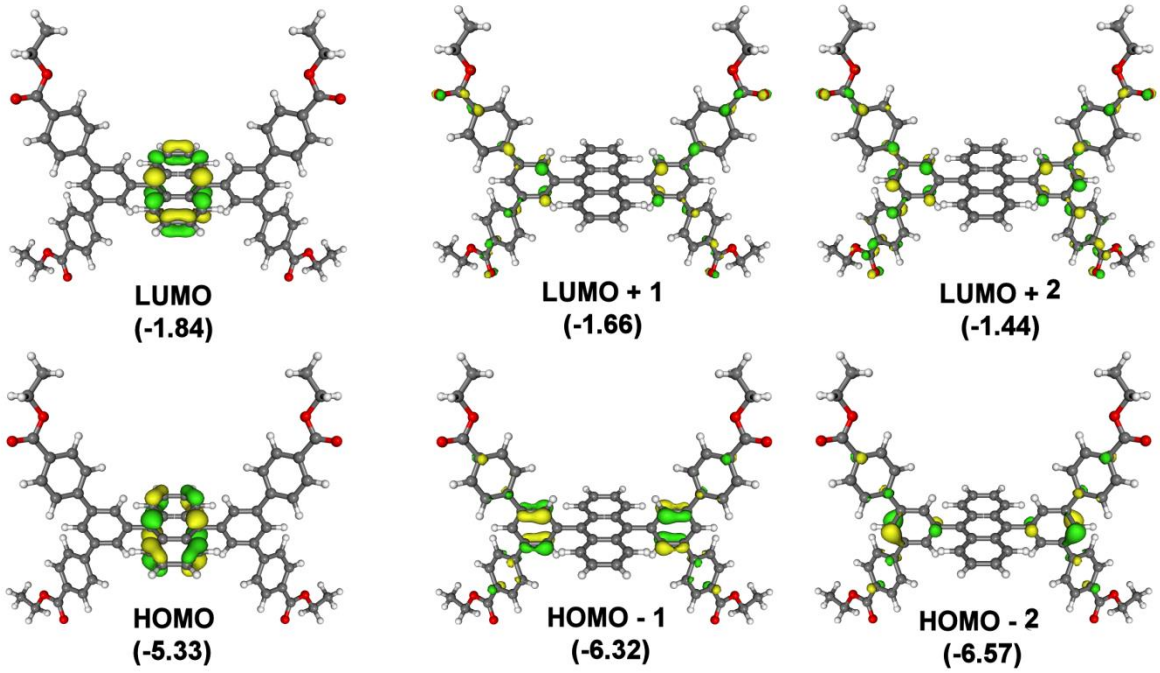

Figure S11: Frontier orbitals of Et_4L^1 and their energy (in eV against vacuum)

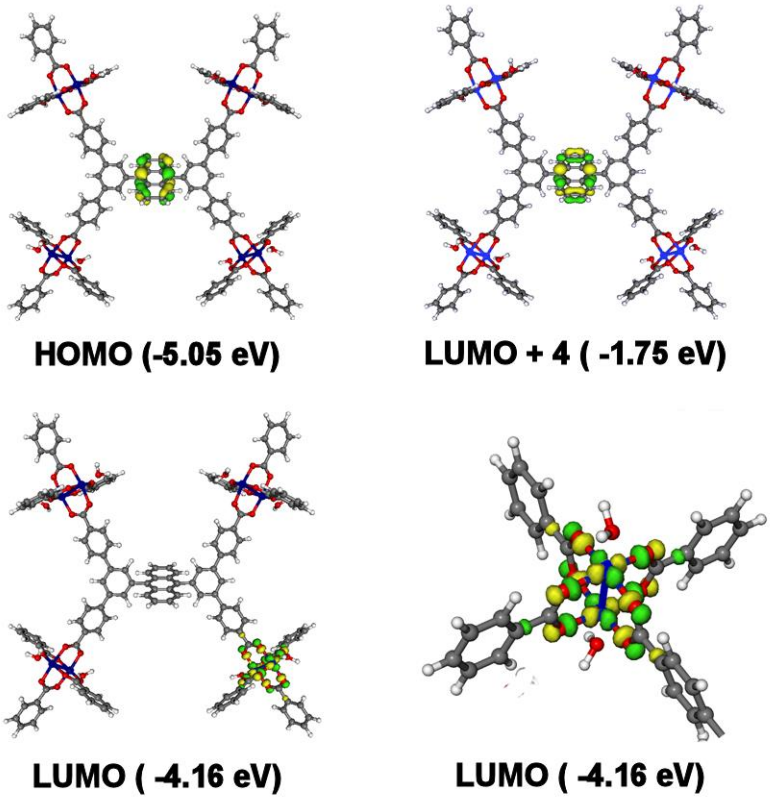

Figure S12: Frontier orbitals of model system for [MFM-170] and their energy (in eV against vacuum)

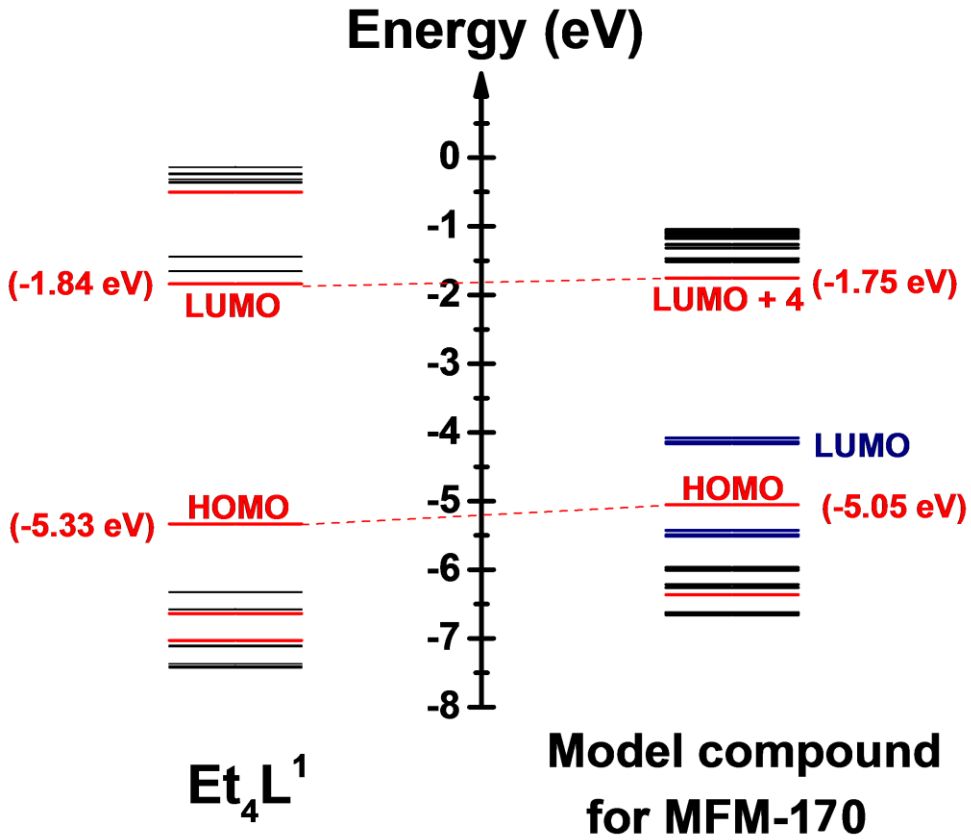

Figure S13: Comparison of the energy of frontier orbitals of Et_4L^1 and of the model system for [MFM-170]. The red levels indicate orbitals primarily confined to the anthracene motif, while blue levels show the Cu-paddlewheel-based orbitals. Note that the LUMO in the model system is Cu-paddlewheel-based which may explain delamination of MFM-170 films upon reduction.

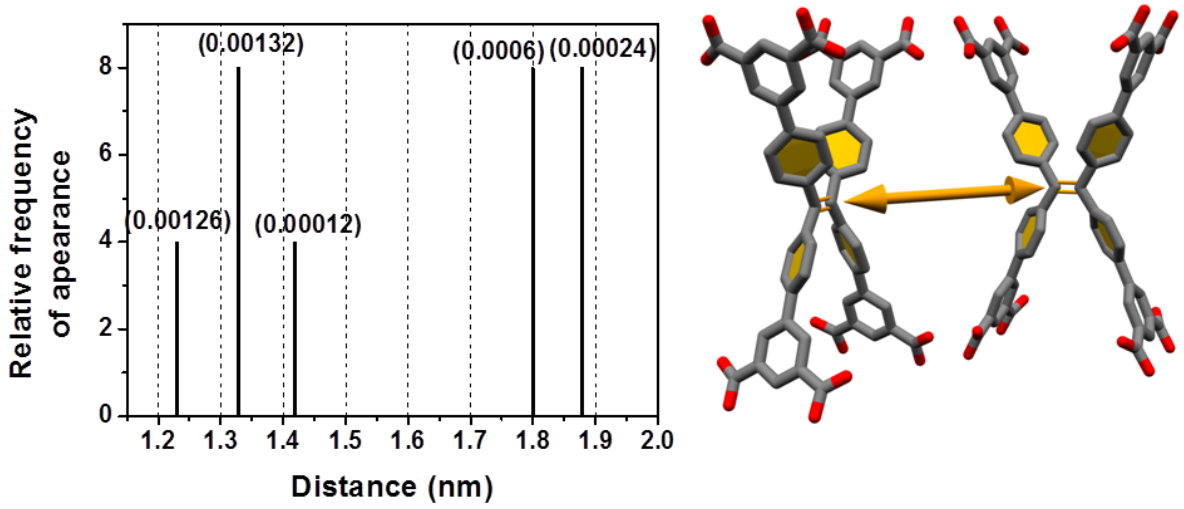

Figure S14: Interatomic distance between two '>C=C<' groups in the MFM-180 framework, as seen in the single crystal structure. The number in parenthesis indicates error limit for distance.

S1. A. G. Slater and A. I. Cooper, *Science*, 2015, **348**.
2. J. R. Long and O. M. Yaghi, *Chemical Society Reviews*, 2009, **38**, 1213-1214.
3. H.-C. Zhou, J. R. Long and O. M. Yaghi, *Chemical Reviews*, 2012, **112**, 673-674.
4. M. Li, D. Li, M. O'Keeffe and O. M. Yaghi, *Chemical Reviews*, 2014, **114**, 1343-1370.
5. S. Yang, A. J. Ramirez-Cuesta, R. Newby, V. Garcia-Sakai, P. Manuel, S. K. Callear, S. I. Campbell, C. C. Tang and M. Schröder, *Nat Chem*, 2015, **7**, 121-129.
6. Z. R. Herm, B. M. Wiers, J. A. Mason, J. M. van Baten, M. R. Hudson, P. Zajdel, C. M. Brown, N. Masciocchi, R. Krishna and J. R. Long, *Science*, 2013, **340**, 960-964.
7. H. Furukawa, K. E. Cordova, M. O'Keeffe and O. M. Yaghi, *Science*, 2013, **341**.
8. Y. Yan, X. Lin, S. Yang, A. J. Blake, A. Dailly, N. R. Champness, P. Hubberstey and M. Schroder, *Chemical Communications*, 2009, DOI: 10.1039/b900013e, 1025-1027.
9. S. Bureekaew, S. Horike, M. Higuchi, M. Mizuno, T. Kawamura, D. Tanaka, N. Yanai and S. Kitagawa, *Nat Mater*, 2009, **8**, 831-836.
10. H. B. Tanh Jeazet, C. Staudt and C. Janiak, *Dalton Transactions*, 2012, **41**, 14003-14027.
11. M. Shah, M. C. McCarthy, S. Sachdeva, A. K. Lee and H.-K. Jeong, *Industrial & Engineering Chemistry Research*, 2012, **51**, 2179-2199.
12. L. Yang, S. Kinoshita, T. Yamada, S. Kanda, H. Kitagawa, M. Tokunaga, T. Ishimoto, T. Ogura, R. Nagumo, A. Miyamoto and M. Koyama, *Angewandte Chemie*, 2010, **122**, 5476-5479.
13. J. Yang, F. Zhao and B. Zeng, *RSC Advances*, 2015, **5**, 22060-22065.
14. M. B. Solomon, T. L. Church and D. M. D'Alessandro, *CrystEngComm*, 2017, **19**, 4049-4065.
15. C.-W. Kung, T. C. Wang, J. E. Mondloch, D. Fairen-Jimenez, D. M. Gardner, W. Bury, J. M. Klingsporn, J. C. Barnes, R. Van Duyne, J. F. Stoddart, M. R. Wasielewski, O. K. Farha and J. T. Hupp, *Chemistry of Materials*, 2013, **25**, 5012-5017.
16. C. R. Wade, M. Li and M. Dincă, *Angewandte Chemie International Edition*, 2013, **52**, 13377-13381.
17. T. L. Easun, J. Jia, T. J. Reade, X.-Z. Sun, E. S. Davies, A. J. Blake, M. W. George and N. R. Champness, *Chemical Science*, 2014, **5**, 539-544.

18. T. L. Easun, J. Jia, J. A. Calladine, D. L. Blackmore, C. S. Stapleton, K. Q. Vuong, N. R. Champness and M. W. George, *Inorganic Chemistry*, 2014, **53**, 2606-2612.
19. A. J. Blake, N. R. Champness, T. L. Easun, D. R. Allan, H. Nowell, M. W. George, J. Jia and X.-Z. Sun, *Nat Chem*, 2010, **2**, 688-694.
20. S. Castellanos, F. Kapteijn and J. Gascon, *CrystEngComm*, 2016, **18**, 4006-4012.
21. C. L. Jones, A. J. Tansell and T. L. Easun, *Journal of Materials Chemistry A*, 2016, **4**, 6714-6723.
22. F.-X. Coudert, *Chemistry of Materials*, 2015, **27**, 1905-1916.
23. J. Szanyi, M. Daturi, G. Clet, D. R. Baer and C. H. F. Peden, *Physical Chemistry Chemical Physics*, 2012, **14**, 4383-4390.
24. R. Hinogami, S. Yotsuhashi, M. Deguchi, Y. Zenitani, H. Hashiba and Y. Yamada, *ECS Electrochemistry Letters*, 2012, **1**, H17-H19.
25. D. M. D'Alessandro, *Chemical Communications*, 2016, **52**, 8957-8971.
26. P. M. Usov, C. Fabian and D. M. D'Alessandro, *Chemical Communications*, 2012, **48**, 3945-3947.
27. D. Zacher, O. Shekhah, C. Woll and R. A. Fischer, *Chemical Society Reviews*, 2009, **38**, 1418-1429.
28. M. Meilikhov, S. Furukawa, K. Hirai, R. A. Fischer and S. Kitagawa, *Angewandte Chemie International Edition*, 2013, **52**, 341-345.
29. M. C. So, S. Jin, H.-J. Son, G. P. Wiederrecht, O. K. Farha and J. T. Hupp, *Journal of the American Chemical Society*, 2013, **135**, 15698-15701.
30. A. Summerfield, I. Cebula, M. Schröder and P. H. Beton, *The Journal of Physical Chemistry C*, 2015, **119**, 23544-23551.
31. Y. Yan, S. Yang, A. J. Blake and M. Schröder, *Accounts of Chemical Research*, 2014, **47**, 296-307.
32. B. Gole, A. K. Bar, A. Mallick, R. Banerjee and P. S. Mukherjee, *Chemical Communications*, 2013, **49**, 7439-7441.
33. F. Moreau, T. Easun, A. Blake and M. Schroder, unpublished work.
34. Z. Wei, W. Lu, H.-L. Jiang and H.-C. Zhou, *Inorganic Chemistry*, 2013, **52**, 1164-1166.
35. A. Laforgue, T. Addou and D. Bélanger, *Langmuir*, 2005, **21**, 6855-6865.
36. E. Biemmi, C. Scherb and T. Bein, *Journal of the American Chemical Society*, 2007, **129**, 8054-8055.
37. O. Shekhah, H. Wang, S. Kowarik, F. Schreiber, M. Paulus, M. Tolan, C. Sternemann, F. Evers, D. Zacher, R. A. Fischer and C. Wöll, *Journal of the American Chemical Society*, 2007, **129**, 15118-15119.
38. C. Munuera, O. Shekhah, H. Wang, C. Woll and C. Ocal, *Physical Chemistry Chemical Physics*, 2008, **10**, 7257-7261.
39. H. K. Arslan, O. Shekhah, J. Wohlgemuth, M. Franzreb, R. A. Fischer and C. Wöll, *Advanced Functional Materials*, 2011, **21**, 4228-4231.
40. A. J. Bard and L. R. Faulkner, *Electrochemical Methods: Fundamentals and Applications*, Wiley VCH, 2nd edn., 2001.
41. A. Paine and R. Loutfy, *Res Chem Intermed*, 1984, **5**, 227-248.
42. N. G. Connelly and W. E. Geiger, *Chemical Reviews*, 1996, **96**, 877-910.
43. Y. Inokuma, M. Kawano and M. Fujita, *Nat Chem*, 2011, **3**, 349-358.
44. C. S. Diercks, Y. Liu, K. E. Cordova and O. M. Yaghi, *Nature Materials*, 2018, **17**, 301-307.
45. S. Creager, C. J. Yu, C. Bamdad, S. O'Connor, T. MacLean, E. Lam, Y. Chong, G. T. Olsen, J. Luo, M. Gozin and J. F. Kayyem, *Journal of the American Chemical Society*, 1999, **121**, 1059-1064.
46. C. E. Check, T. O. Faust, J. M. Bailey, B. J. Wright, T. M. Gilbert and L. S. Sunderlin, *The Journal of Physical Chemistry A*, 2001, **105**, 8111-8116.
47. P. Ugliengo, D. Viterbo and G. Chiari, *Zeitschrift für Kristallographie*, 2010, **207**, 9-23.
48. U. Varetto, *Journal*.